CHAPTER 3

Analytical Development of 1:6-Scale Shaking Table Model

3.1 Introduction

The primary goals of the shaking table experiments were to demonstrate the effectiveness of the rope devices to reduce overall story drift and reduce residual deformations for a two-story office structure in a scaled experiment. This chapter summarizes the analyses used to develop a valid prototype moment frame and a scaled model frame that properly represents the prototype frame.

The method used to develop a valid prototype involved first considering current building code based design of a moment frame for the prototype building. A preliminary frame was designed using the equivalent lateral force procedures outlined in FEMA (2003a), as detailed in Section 3.3. A nonlinear response history analysis of the prototype moment frame was evaluated using DRAIN-2DX (1998), referred to herein as DRAIN. Based on a parametric study conducted using DRAIN, optimized rope device parameters were established. The DRAIN finite element model used for all analyses is detailed in Section 3.4, and the parametric study of the prototype is detailed in Section 3.5.

The scale for the model was based on the full-scale prototype frame. Characteristics of the shaking-table equipment and limitations related to rope construction provided a range of possible alternatives for the size of the model to be used for the shaking table experiments. Two primary factors controlled the scale of the shaking table experiment. The length scale was limited to a maximum of 1:5 by the plan dimensions of the shaking table, and a minimum of 1:8 by the minimum length requirements for the ropes. It was determined that using the largest possible scaled model was desirable for a variety of reasons, including simplification of frame member construction and detailing. Based on the shaking-table ballast tests reported in Appendix B, a 1:5.78-scale frame was determined to be the largest model that could be tested using the available shaking table. Standard steel tube sections, appropriate for modeling the bending stiffness of the prototype steel frame at a 1:5.78-scale, were available. Based on these considerations, a single-bay, two-story, 1:5.78-scale tube steel model was chosen for the shaking table experiment. The scale frame is referred to from this point forward as a 1:6-scale frame.

A relationship between dynamic response parameters of a 5-bay, 2-story prototype steel moment frame, constructed using wide-flanged steel members, to the dynamic response characteristics of a 1:6-scale, single-bay, 2-story tube steel frame was required. Because of the uncertainty involved with directly scaling the prototype to a 1:6-scale model, an intermediate full-scale tube steel frame was first considered and analyzed using DRAIN. The analysis of the intermediate frame and a comparison of the dynamic response of the intermediate frame to the prototype are provided in Section 3.6. The 1:6-scale frame was then proportioned based on similitude with the intermediate frame and analyzed using DRAIN. The analysis and a comparison of the response of the scaled moment frame with the prototype frame are detailed in Section 3.7.1. Finally, scaling the prototype rope device, selected in the parametric study of the full-scale frame, was conducted and is presented in Section 3.7.2.

For reference, the moment frames discussed in this Chapter are listed with the number of bays, and member sizes, and nominal yield stress in Table 3.1.

Table 3. 1: Moment Frames Used for the Development of the 1:6-Scale Frame

Designation	# of Bays	Column Sizes	Beam Sizes	Yield Stress (ksi)
Full-Scale Prototype	5	W18x71	W18x50	50
Intermediate Moment Frame	1	HSS16x8x5/16	HSS14x4x3/8	50
1:6-Scale Frame	1	HSS1-3/4x1-3/4x5/16	HSS1-1/2x1-1/2x1/8	50

3.2 STRUCTURAL DESCRIPTION OF THE PROTOTYPE BUILDING

The prototype building considered was a two-story steel frame office building. A plan of the typical floor and roof framing is shown in Figure 3.1. The lateral force resisting system consists of special steel moment frames along the four perimeter walls. This study concentrated on the moment frame located along column line 1: an elevation of the moment frame is illustrated in Figure 3.2. All moment frame members were bent about the strong axis, or “X” axis, as defined in AISC (2005a). Beams-to-column connections were considered fully-rigid, and columns were fixed at the base. Panel zone deformations were not included in drift calculations. All columns not included in the perimeter moment frames were idealized as being pinned at the top and bottom, and therefore did not contribute lateral stiffness to the lateral force resisting system.

The floor system was assumed to be made up of a normal weight concrete slab on composite steel deck. The floor live load was 50 psf. The dead load of the floor system was 75 psf, with 10 psf added for moveable partitions, and 10 psf added for lighting, ceiling, and mechanical, electrical, and plumbing systems. The total dead load is therefore 95 psf at the floor. The cladding weight at the full perimeter was taken as 30 psf. A 125-psf storage load was assumed to act over 15 percent of the total floor area. Twenty-five percent of the storage load was used for the seismic dead load calculations.

The roof system is metal deck on open web steel joists with rigid insulation. The roof dead load is 30 psf.

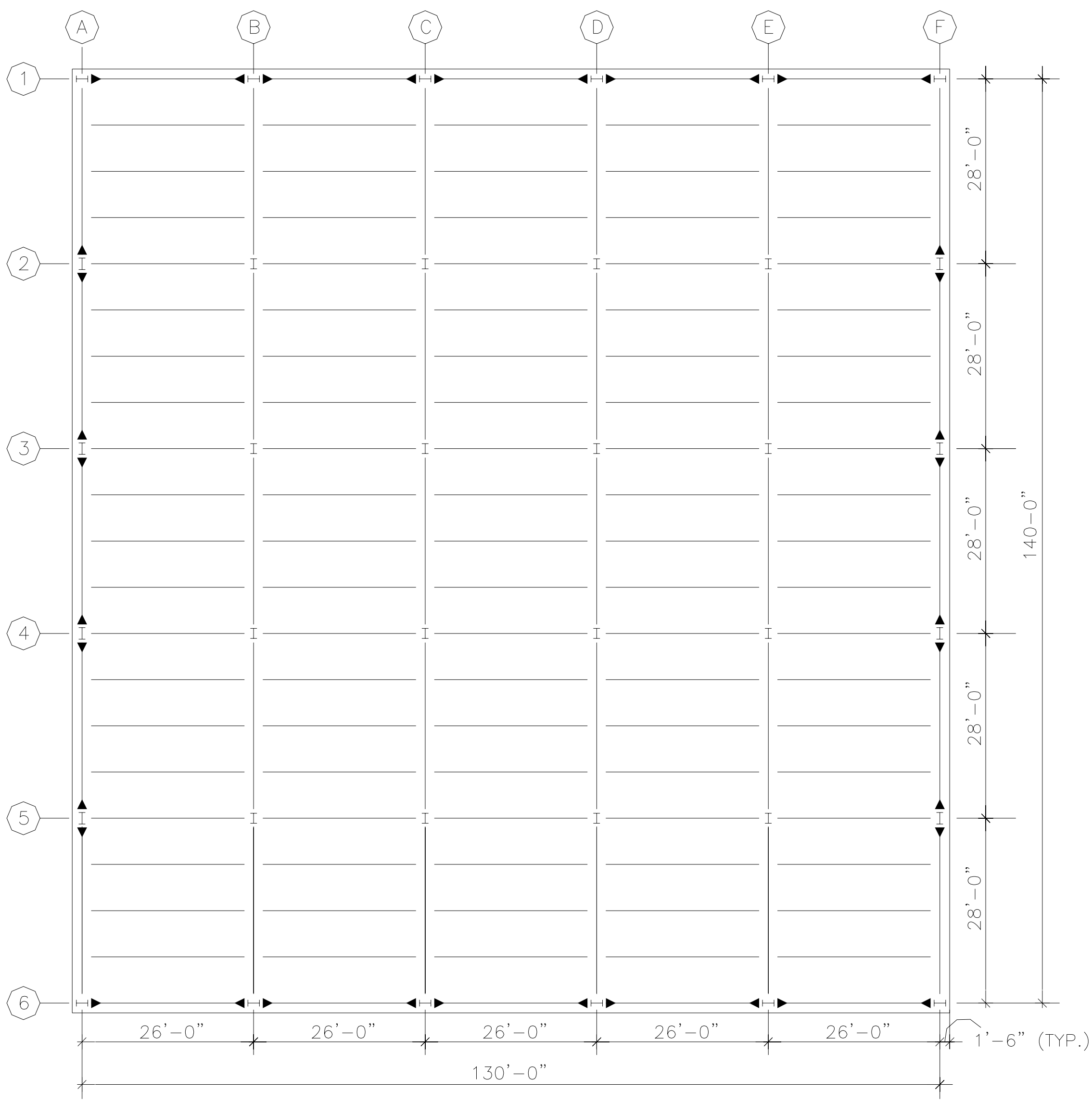

Figure 3. 1: Prototype Building: Floor/Roof Framing Plan

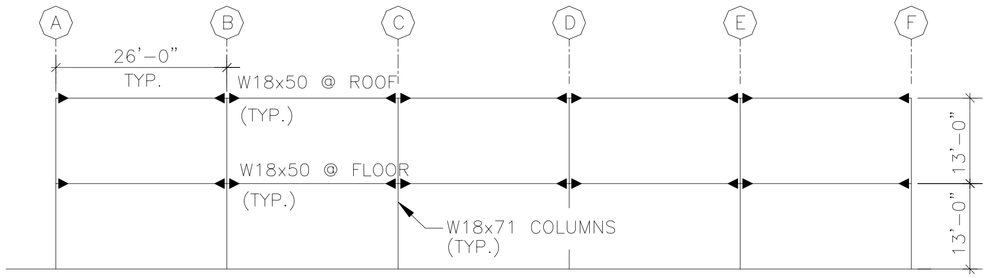

Figure 3. 2: Prototype Building: Typical Moment Frame Elevation at Grid Lines 1 and 6

The total building weight estimates used for the seismic analysis are shown in Table 3.2, based on the given live and dead loads. The table lists dead loads, storage loads, and total loads used for the seismic calculations. Total building weight, W, used for seismic calculations included dead and 25% of the storage load.

Charleston, South Carolina was chosen to develop a lateral force resisting system based on current building code provisions. Due to extremely large seismic events, which have occurred in Charleston, mapped design spectral acceleration, provided in FEMA (2003a), are larger than in any other highly populated areas in the CEUS. In addition to the risk of a large event occurring in Charleston, there has been a lack of perceived risk due to the large interval between seismic events. The last major earthquake to occur in Charleston was approximated to be magnitude 7.3 on the moment magnitude scale (Talwani et al., 2001), and occurred in 1886. Since that time, no seismic event approaching this level has been recorded, causing the risk of seismic events to be neglected until the development of recent building codes, resulting in a large building stock with inadequate seismic detailing. Since the ropes are being considered as drift control devices which add limited additional force requirements to structural systems, consideration for use in a retrofit solution follows naturally. Therefore Charleston was determined to be an appropriate geographic locale based on large spectral acceleration values in current code requirements and the potential for use of ropes as retrofit solutions.

Table 3. 2: Building Loads for Seismic Calculations

Level	**Dead Load**		**25% Storage Load**		**Total**	
	Story (kips)	**Accum. (kips)**	**Story (kips)**	**Accum. (kips)**	**Story (kips)**	**Accum. (kips)**
Roof	728	728	0	0	728	728
1	2022	2750	90	90	2112	* 2840

* Indicates total estimated weight (W) of building used for seismic calculations

3.3 EQUIVALENT LATERAL FORCE PROCEDURE

For the seismic calculations, the building was assigned to Seismic Use Group I and Site Class D, and the importance factor, I, was taken as 1.0. Given the site, Charleston, South Carolina, the short period and one second period mapped spectral accelerations values are:

$$S_S = 1.63 \text{ g} \tag{3-1}$$

$$S_1 = 0.46 \text{ g} \tag{3-2}$$

Site coefficient values, obtained from FEMA (2003a) Tables 3.3-1 and 3.3-2 for Site Class D, are:

$$F_a = 1.00$$

$$F_v = 1.58$$

Maximum considered spectral acceleration values are calculated using FEMA (2003a) Equations 3.3-1 and 3.3-2:

$$S_{MS} = S_S F_a = (1.63 \text{ g})(1.00) = 1.63 \tag{3-3}$$

$$S_{M1} = S_1 F_v = (0.46 \text{ g})(1.58) = 0.73 \tag{3-4}$$

Design Spectral acceleration values are calculated using FEMA (2003a) Equations 3.3-3 and 3.3-4:

$$S_{DS} = (2/3)S_{MS} = (2/3)(1.63) = 1.09 \tag{3-5}$$

$$S_{D1} = (2/3)S_{M1} = (2/3)(0.73) = 0.49 \tag{3-6}$$

Based on FEMA (2003a) Tables 1.4.-1 and 1.4-2 and the calculated design spectral values, the structure is in Seismic Design Category D. Special moment frames make up the lateral force resisting system with a response modification factor, R, equal to 8, and a drift amplification factor, C_d, equal to 5.5, from FEMA (2003a) Table 4.3-1.

FEMA (2003a) Equation 5.2-6 was used to determine the approximate period of vibration:

$$T_a = C_r h_n^x = (0.028)(26\text{ft})^{0.8} = 0.38 \text{ seconds} \tag{3-7}$$

where h_n is the height of the structure in feet, and values for C_r and x are provided based on structure type in FEMA (2003a) Table 5.2-2.

FEMA (2003a) allows for the use of a more precisely calculated fundamental period of a structure, determined through a properly substantiated process. However, for base shear calculations used for strength requirements, the calculated fundamental period is limited as follows:

$$T_1 \leq C_u T_a = (1.4)(0.38) = 0.53 \text{ seconds} \tag{3-8}$$

where T_1 is the fundamental period of the structure determined using a properly substantiated process, and the coefficient for the upper limit on the calculated period, C_u, is provided in FEMA (2003a) Table 5.2-1. The fundamental period of the frame resulting from this procedure was eventually determined using the elastic modal analysis formulation of DRAIN and is equal to 0.70 seconds. The DRAIN frame model definition is described in Section 3.4.1. Since the calculated fundamental period was greater than 0.53 seconds, C_uT_a was used for the determination of the seismic response coefficient that follows.

The total seismic base shear was determined using FEMA (2003a) Equation 5.2-1:

$$V = C_s W \tag{3-9}$$

where W is the total weight of the structure in kips, and C_s is the seismic response coefficient based on the fundamental period of the structure. The maximum value of C_s was calculated using FEMA (2003a) Equation 5.2-2:

$$C_s = \frac{S_{DS}}{(R/I)} = \frac{1.08}{(8.0/1.0)} = 0.135 \tag{3-10}$$

C_s need not be greater than the value calculated using FEMA (2003a) Equation 5.2-3:

$$C_s = \frac{S_{D1}}{T(R/I)} = \frac{0.49}{0.53(8.0/1.0)} = 0.114 \tag{3-11}$$

The value for total seismic base shear was calculated using the maximum value for C_s=0.114, and W=2,840 kips, and is 323 kips.

The total base shear was distributed to the roof and floor diaphragms based on FEMA (2003a) Equations 5.2-10 and 5.2-11:

$$F_x = C_{vx} V \tag{3-12}$$

$$C_{vx} = \frac{w_x h_x^k}{\sum_{i=1}^{n} w_i h_i^k} \tag{3-13}$$

where k= 0.75 + 0.5 T = 0.75 + (0.5)(0.53) = 1.01. Table 3.3 lists the values for story weight, w_x, story height, h_x, story distribution factor, C_{vx}, and the resultant equivalent lateral force at each diaphragm level, F_x. Note that the forces listed represent total design forces for the entire building structure. These values were divided by 2 for design of a single frame.

Table 3. 3: Vertical Distribution of Base Shear (Strength Considerations)

Level *x*	**w_x (kips)**	**h_x (ft)**	**C_{vx}**	**F_x (kips)**	**V_x (kips)**
Roof	728	26	0.41	132	132
1	2112	13	0.59	191	323

The five-bay, N-S frame was modeled using the software RISA (2005). The structure was analyzed with the lateral forces in Table 3.3, and applicable dead, live, and roof live loads using load combinations from IBC 2003, Section 1605.2.1, listed in Table 3.4:

Table 3. 4: IBC 2000 Basic Load Combinations

IBC Equation Designation	**Load Combination**
16-1	1.4D
16-2	1.2D + 1.6L + 0.5(Roof)
16-3	1.2D + 1.6(Roof) + (0.5L or 0.8W)
16-4	1.2D + 1.6W + 0.5L + 0.5(Roof)
16-5	1.2D + 1.0E + 0.5L+ 0.2S
16-6	0.9D + (1.0E or 1.6W)

Using the member size optimization feature of RISA (2005), W14x53-A992 sections were selected for all columns and W18x35-A992 sections were selected for all beams. The minimum yield stress of the members was taken as 50 ksi as specified in ASTM-A992. The steel sections were checked for adequacy based on the strength and stability requirements of AISC (2005a), and were found to be acceptable. Based on the drift criteria, these sizes resulted in a frame that was too flexible. Sizes were increased to W18x71-A992 sections for all columns and W18x50-A992 sections for all beams. The relative size of the girders with respect to the columns ensures that plastic hinge formation occurs in the girders, as required in the steel seismic provisions, AISC (2005b).

Drift was re-calculated based on the computed fundamental period. Section 5.2.6 of FEMA (2003a) allows drift calculations using T_1 without the upper limit, C_uT_a. The fundamental period of the frame with the updated beam and column sizes was determined to be 0.70 seconds, resulting in a seismic response coefficient calculated as follows:

$$C_s = \frac{S_{D1}}{T(R/I)} = \frac{0.49}{0.70(8.0/1.0)} = 0.085 \tag{3-14}$$

The value for total seismic base shear for drift considerations was determined with $C_s = 0.085$ and W = 2,840 kips, and is 242 kips. The value for k, used to determine C_{vx}, calculated above, is 1.01, slightly changing the vertical distribution of base shear. Base shear was calculated based on FEMA (2003a), Equations 5.2-10 and 5.2-11. Table 3.5 lists the values for story weight, w_x, story height, h_x, story distribution factor, C_{vx}, and the resultant equivalent lateral force at each diaphragm level, F_x, for drift calculations. These values were divided by 2 for analysis of a single frame.

Table 3. 5: Vertical Distribution of Base Shear (Drift Considerations)

Level *x*	**w_x (kips)**	**h_x (ft)**	**C_{vx}**	**F_x (kips)**	**V_x (kips)**
Roof	728	26	0.42	102	102
1	2112	13	0.58	140	242

The model was analyzed with RISA-3D using updated steel sections and story shears. Roof drift and floor drift were calculated based on FEMA (2003a) Equation 5.2-15:

$$\delta_x = \frac{C_d \delta_{xe}}{I} \tag{3-15}$$

where δ_{xe} is the story drift calculated by elastic analysis, and C_d is the deflection amplification factor, equal to 5.5. The importance of P-Delta effects on drift was evaluated based on Section 5.2.6.2 of FEMA (2003a). The stability factor was calculated as follows:

$$\theta = \frac{P_x \Delta I}{V_x h_{sx} C_d} = \frac{(2840\text{kips})(3.3\text{in.})(1.0)}{(242\text{kips})(156\text{in.})(5.5)} = 0.045 \leq 0.1 \tag{3-16}$$

Since the value is less than the limit of 0.10, P-Delta effects were neglected in the analysis. Resulting calculated roof and floor drifts, and allowable roof and floor drifts, are listed in Table 3.6. The code allowable story drift is equal to 2%. The roof story drift was within that limit and the floor drift was considered to be acceptably close to the 2% limit.

Table 3. 6: Drift Analysis Results

Level, *x*	**Elastic Drift, δ_{xe} (in.)**	**Amplified Drift, δ_x (in.)**	**Percent Story Drift (%)**
R	1.1	6.1	1.8
1	0.6	3.3	2.1

The updated steel sections (W18x71-A992 columns and W18x50-A992 beams) were checked for adequacy based on the strength and stability requirements of AISC (2005a), and found to be acceptable. Therefore, all prototype columns and beams are W18x71-A992 and W18x50-A992, respectively.

3.4.1 DRAIN-2DX MODEL DESCRIPTION

All two-dimensional, nonlinear response history and static push-over analyses used to develop the scale model frame were conducted using DRAIN. Description of the functionality of the use of these elements was adapted from Prakash, et al. (1993). The general form of the model was adopted from Charney (2004). A general, two-story frame description is presented. Four DRAIN element types available were used as listed in Table 3.7 with corresponding element descriptions from DRAIN and usage descriptions for this study. An element usage diagram is presented in Figure 3.3.

Table 3. 7: Drain-2DX Elements Used

Element	Element Description	Element Usage
Type-01	Elastic Truss Element	Leaner Frame Columns
Type-02	Beam-Column Element	Moment Frame Beams and Columns
Type-04	Connection Element	Nonlinear Hinges at Member Ends
Type-09	Compression/Tension Link Element	Ropes

3.4.2 MOMENT-FRAME BEAM AND COLUMN ELEMENTS (TYPE-02)

For all moment-frame beams and columns, Type-02 elements were used. Type-02 elements are elastic beam-column elements, for which material properties including Young's modulus, Poisson's ratio and cross-sectional member properties, including bending stiffness, gross area, and shear area, are defined by the user. Additionally, the Type-02 element formulation allows for a nonlinear plastic hinging definition at the member ends. In lieu of this option, an alternative method of defining hinging behavior was used and is discussed in Section 3.4.3. Shear and axial deformations were included for both columns and beams. However, axial deformation was inhibited in all girders by defining an increased cross-sectional area, approximating the addition of axial stiffness to the section due to the floor slab.

Bending stiffness due to composite beam-slab interaction was neglected for several reasons. Practical design of steel moment frames commonly neglects the contribution of the slab due to the inaccuracies encountered when modeling the concrete contribution at the hinge location, particularly when the concrete is in tension. Additionally, detailing confinement reinforcing is not common in practice. Without confinement reinforcing at the hinge location, the concrete does not provide reliable force transfer through multiple cycles of loading subsequent to concrete cracking.

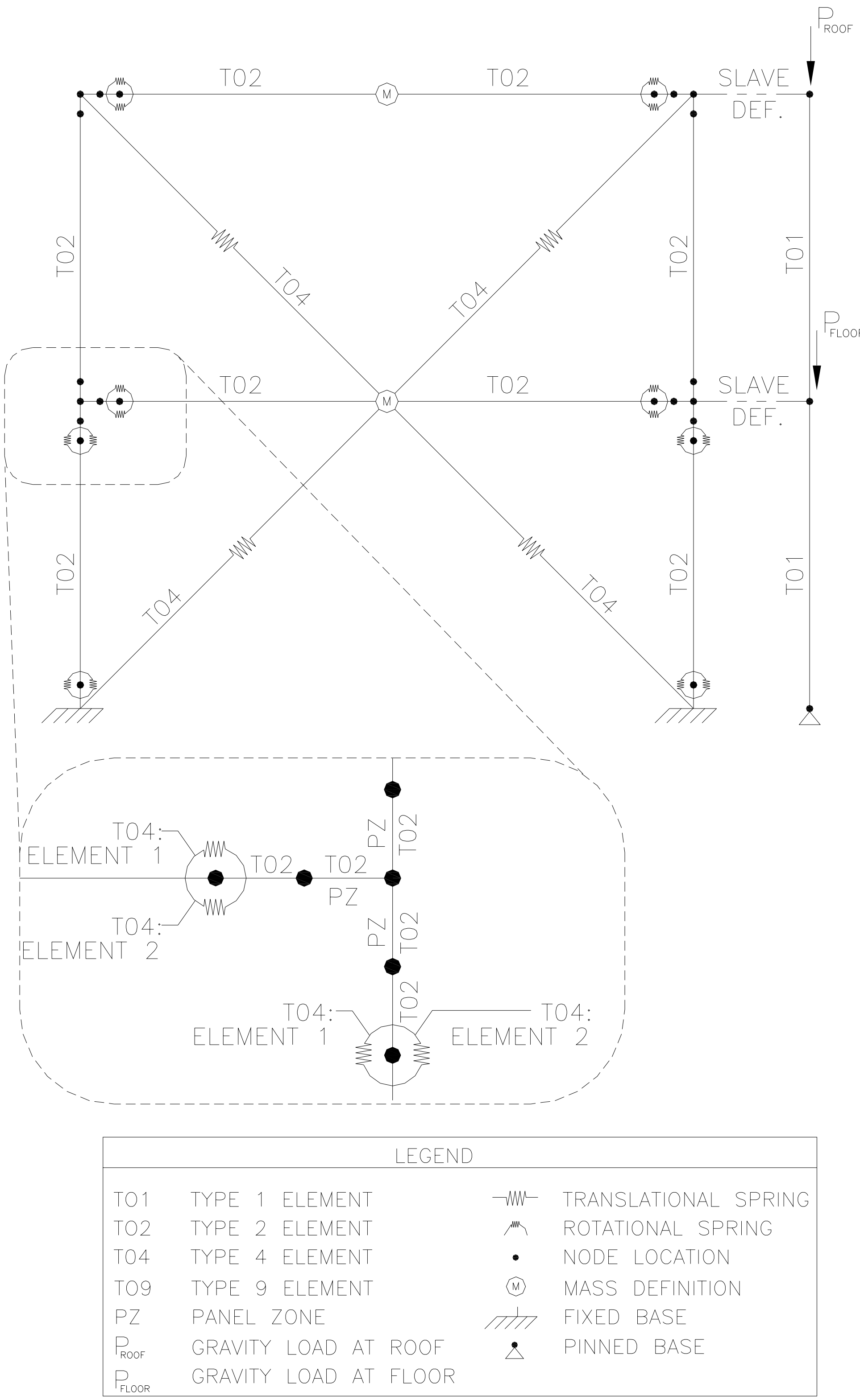

Figure 3. 3: Drain-2DX Element Usage Diagram

3.4.3 Nonlinear Hinge Elements at Member Ends (Type-04)

Hinging responses at member ends were modeled using a combination of two Type-04 elements. The element connectivity at a typical node is illustrated in Figure 3.3. Two Type-02 beam elements were modeled at each side of the node where hinging was assumed to occur. A master/slave node definition was defined at the node, such that the vertical and horizontal translations of the slave node were fixed to the horizontal and vertical translations of the master. In the absence of Type-04 elements, the rotational degree of freedom at the node would be free, allowing the slaved node to rotate independently of the master node rotation. Each Type-04 element was defined by a moment-rotation relationship in which initial stiffness, yield moment, and post-yield stiffness were input. An illustration of the response definitions for the Type-04 elements and the combined response of the two are shown in Figure 3.4. An example calculation of the parameters used for hinge element definitions is provided in Appendix C.

Material properties of steel frame members for the development of hinge elements included elastic stiffness, yield point, and strain hardening. The elastic stiffness was assumed to be Young's modulus, 29,000 ksi. The yield point was assumed to occur at 110% of the minimum specified yield point, or 55 ksi for A992 steel and 50 ksi for A500 steel and of HSS members. Strain hardening was approximated to occur at 3% of Young's modulus.

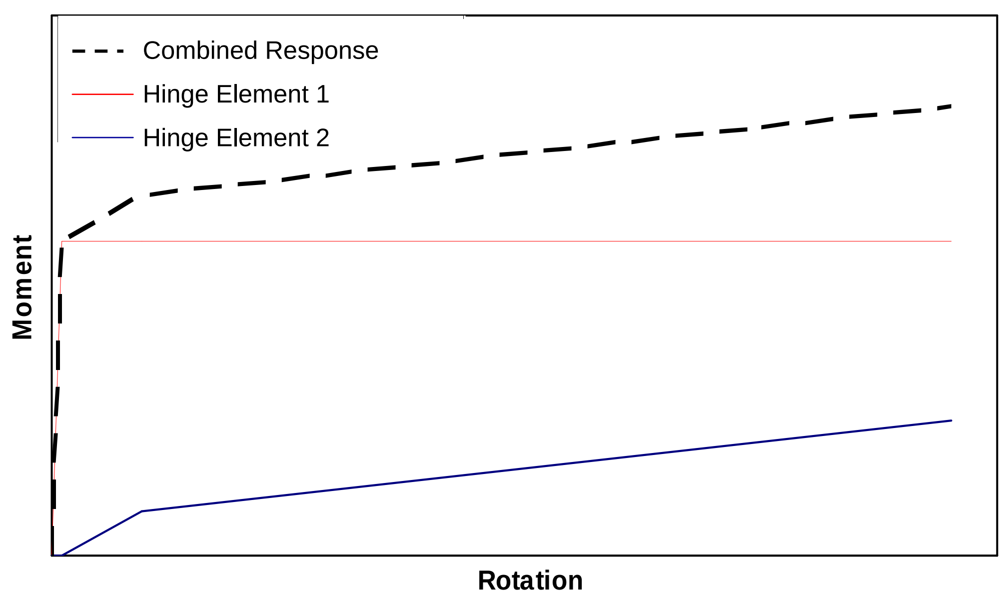

Figure 3. 4: General Hinge Response Definition Using Type-04 Elements

3.4.4 ROPE ELEMENTS (TYPE-09)

Rope device response was modeled using Type-09 elements, which allow for a tri-linear axial response definition. The element formulation also allows for inelastic unloading. However, since the inelastic unloading results in residual deformation, which was not observed in rope testing, elastic unloading was used for the rope definition. The theoretical response of Type-09 elements used in this study is illustrated in Figure 3.5. The rope response was defined by providing three stiffness values (k1, k2, and k3) and two transition displacement values (u1 and u2). The tri-linear stiffness definition allows for a loading response that closely matches the loading response observed in rope testing. Figure 3.6 shows the comparison of the response of a 1-in. nominal diameter rope, modeled in DRAIN, overlaying the response of a 1-in. nominal diameter Amsteel II rope, recorded during the full-strength rope tests documented in Chapter 3. The fit for the loading portion of the experimental data was adequate, while the unloading portion of the experimental response curve was not matched. Since energy dissipation exhibited by the ropes was minor during initial rope testing, this model was determined to be acceptable. Further, the resulting maximum base shear, displacement, and acceleration will be conservatively calculated using this model.

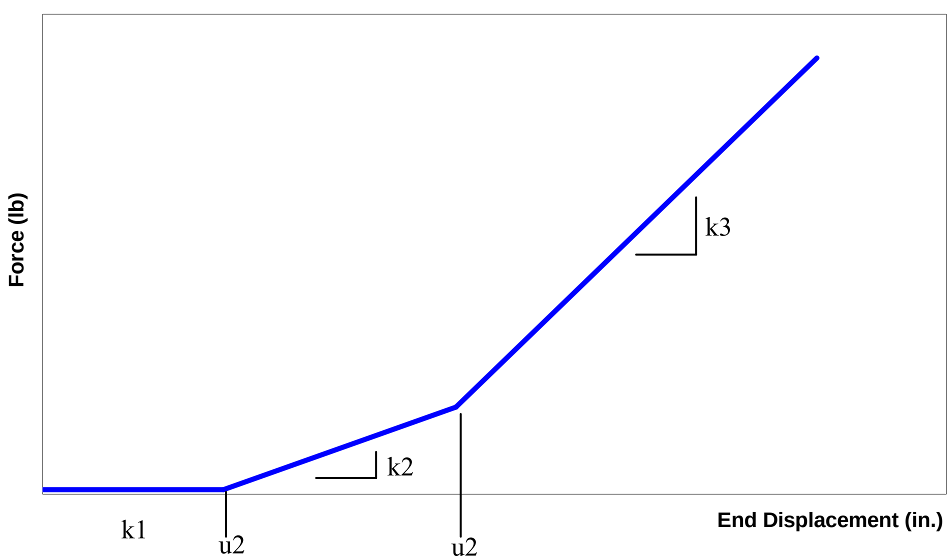

Figure 3. 5: Rope Response Definition Using Type-09 Elements

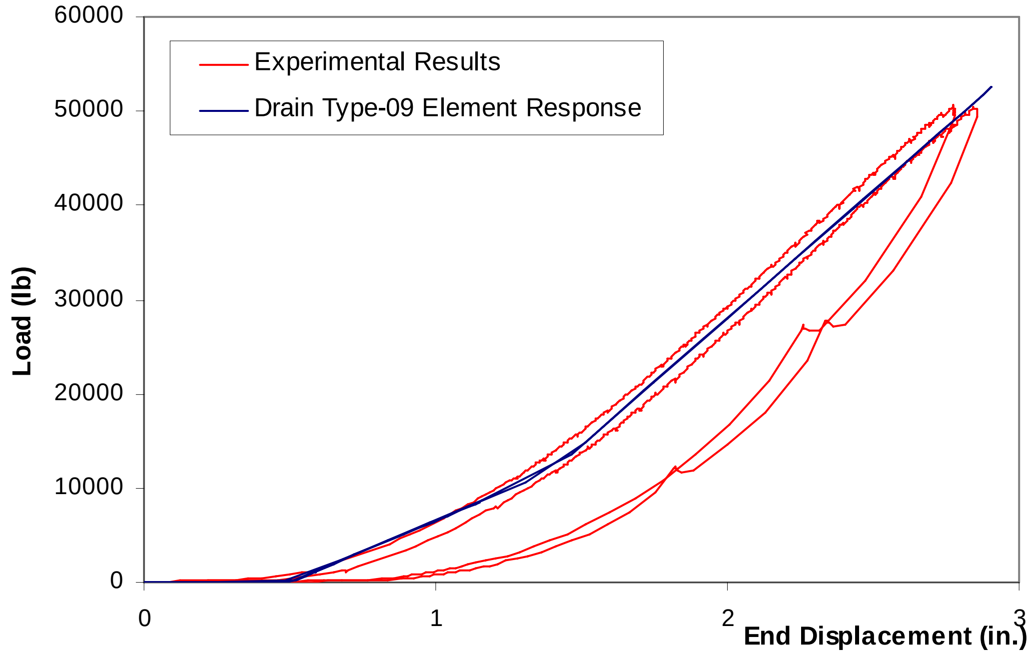

Figure 3. 6: Type-09 Element Response Comparison with Experimental Data

3.4.5 P-Delta Considerations

The moment contributed to the frame through gravity loading acting on the deformed frame, commonly referred to as P-Delta moment magnification, was also included in the DRAIN analysis. A single-column auxiliary frame composed of rigid links was created using standard DRAIN truss elements, Type-01. The truss elements were defined with an effectively infinite axial stiffness. The auxiliary frame was connected to the moment frame at the roof and floor diaphragm levels, using slaving definitions. Translational degrees of freedom at the nodes of the auxiliary frame were slaved to the corresponding moment-frame nodes, while the rotational degree of freedom was not. This allowed the moment frame to deflect without influence from the stiffness of the auxiliary frame. Gravity loading, equal to the story weight, was applied at the floor and roof diaphragm levels. Progressive loading, provided for in DRAIN, allows story loading to be applied prior to conducting response history simulations, and was utilized during the analyses.

3.5 PROTOTYPE PARAMETRIC STUDY

The purpose of the prototype frame parametric study was to determine optimum rope parameters, balancing the maximum reduction in drift with minimal increase to base shear of the prototype moment frame. Two rope parameters were varied: the number of ropes and the size of the initial gap required for the frame to move prior to engaging the ropes.

A suite of six ground motions, separated into near and far field events, was used for this parametric study. Four recorded ground-motion acceleration records and two artificial ground-motion acceleration records, developed to contain acceleration at specific frequencies were included. The artificial ground motions are termed "synthetic". The mean pseudo-spectral acceleration values were then scaled based on FEMA (2003a), Section 5.4.2.1, which requires ground motions to be scaled such that the mean value of the five-percent-damped spectra not be less than the design response spectrum for all values between 20% and 150% of the fundamental period, T_1. For the near-field events, it was determined that scaling the mean spectrum to match the design spectrum at 20% of the fundamental period was excessively conservative. A more reasonable lower limit was determined to be 32% of the fundamental frequency, which encompasses the second-mode resonant period of vibration. The resulting variation to the code provisions was determined to be reasonable. The resulting scaled mean response spectrum for the near-field suite of ground motions is plotted with the design response spectrum in Figure 3.7. Scaling of the mean pseudo-spectral values of the far-field events per FEMA (2003a) was found not to be overly conservative and no variation to the code provisions was required. The scaled mean response spectrum for the far-field suite of ground motions is plotted with the design response spectrum in Figure 3.8. First and second resonant periods of vibration for the prototype moment frame, T_1 and T_2, are also indicated in Figures 3.7 and 3.8 for reference. Ground motions used are listed with corresponding scale factors in Table 3.8.

Table 3. 8: Ground Motion Scaling Factors

Ground Motion Description	Scaling Factor	Classification
Northridge	1.03	Near Field
Kobe	0.31	Near Field
Near Field – Synthetic	1.74	Near Field
Imperial Valley	1.67	Far Field
Chile	1.14	Far Field
Far Field - Synthetic	0.82	Far Field

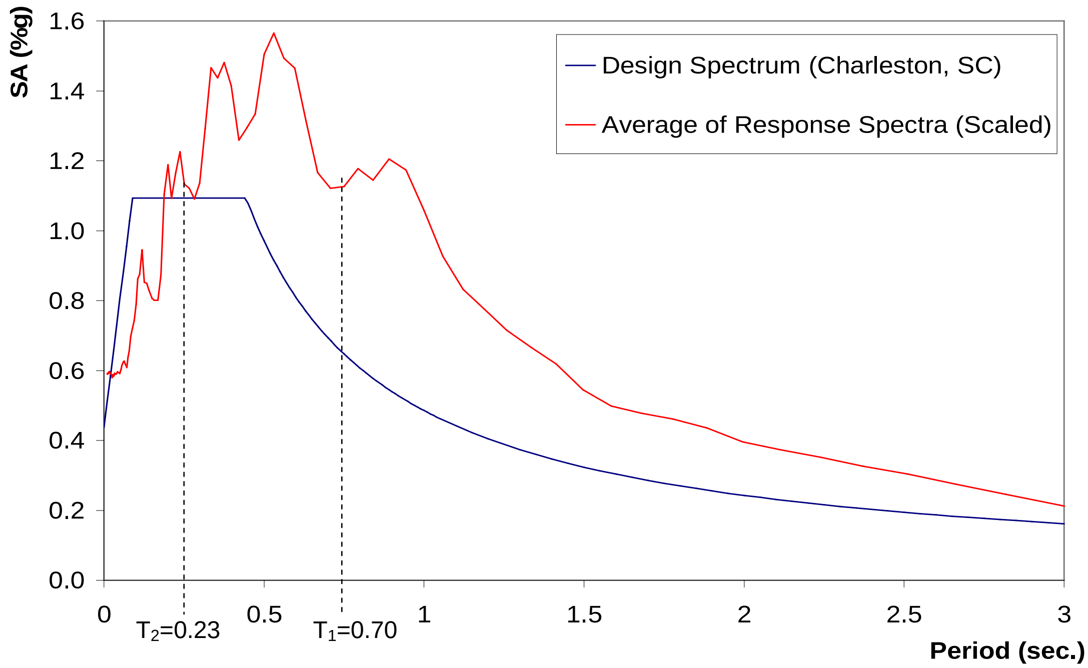

Figure 3. 7: Average Scaled Response Spectrum – Near Field

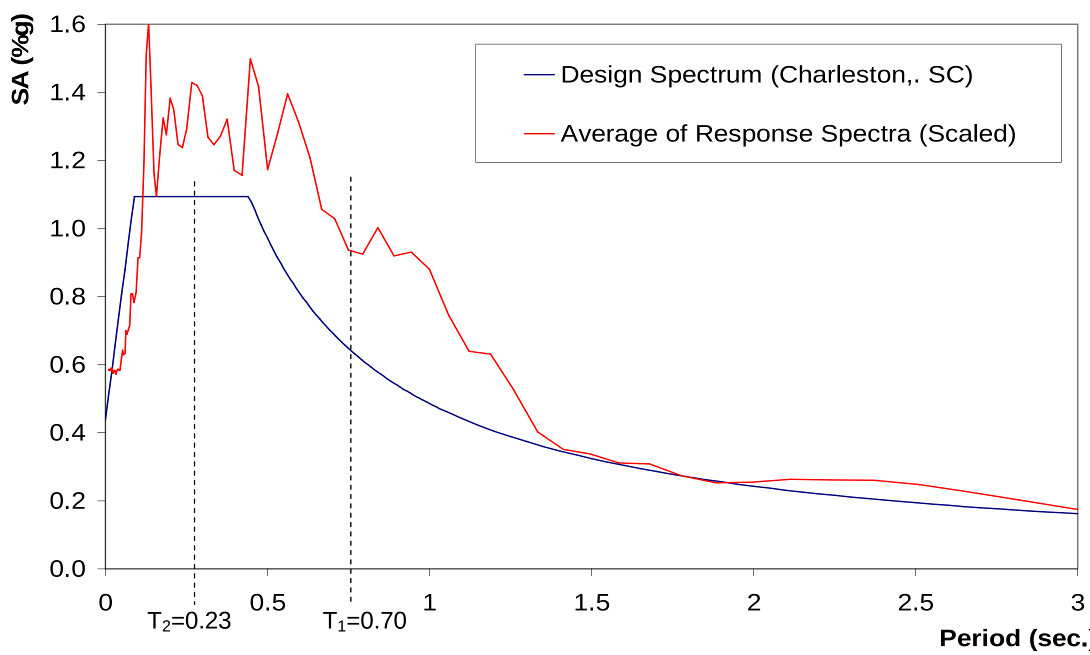

Figure 3. 8: Average Scaled Response Spectrum – Far Field

A series of nonlinear response history analyses was conducted using DRAIN. Inherent damping of the frame was defined in DRAIN using mass and stiffness proportional damping, resulting in equivalent viscous damping of approximately 2%. Damping was only defined for elements with linear-elastic property definitions. Stiffness proportional damping coefficients for elements with non-linear response characteristics were set to zero. The prototype frame without ropes was analyzed using the six scaled ground motion records as base acceleration input. Type-09 elements were then added to the model in the configuration shown in Figure 3.3. The number of ropes was varied from three to six, and the initial gap in the rope was varied from 0.2 in. to 1.0 in., at 0.2 in. increments. Each rope variation was analyzed using the six scaled ground motion records as base acceleration input. A comparison of response parameters of interest, including second floor and roof maximum and residual drifts, maximum base shear, and maximum rope force for frame analyses without ropes, and for analyses where four, five, and six ropes were modeled, are listed in Tables 3.9 and 3.10 for near field and far field events, respectively.

Results of all simulations were considered to determine the optimal rope configuration. Average maximum overall and maximum drift reductions were compared against corresponding increases in base shear. It was determined that the response of three ropes with an initial gap of 0.4 in. provided the optimum results, and was used as the target prototype rope element response. It should be noted that the minimum break strength for three, 1-in.-diameter ropes is 165 kips, which is less than the maximum rope force calculated for some of the simulations. As noted before, and for simplicity, the response curve was based on an eight-foot, 1-in.-diameter rope response. By increasing the length of the ropes, the same response curve could be achieved using a greater number of ropes. Therefore, the capacity of the rope device could be increased as required, without changing the overall response modification to the frame by adding the rope devices.

Roof drift history results of the frame without ropes and of the frame with the selected prototype rope device for each ground motion input are illustrated in Figures 3.9 through 3.14. Plastic hinging and residual deformation were observed in the frames for all simulations. The improvement in overall residual and roof drift varies based on the ground motion considered. Results from simulations using near field ground motion events were considerably better than results of simulations using far field ground motion events.

Table 3. 9: Near Field Event Results of Parametric Rope Analyses

	Frame Only	3 Ropes					4 Ropes					5 Ropes				
Initial Gap (in.)	n/a	0.2	0.4	0.6	0.8	1.0	0.2	0.4	0.6	0.8	1.0	0.2	0.4	0.6	0.8	1.0
Northridge																
Max. Rope Force (kips)	n/a	110	106	114	118	118	150	122	126	134	134	210	150	136	144	146
Max. Roof Drift (in.)	8.25	5.11	5.17	5.75	6.30	6.72	5.14	5.05	5.36	5.91	6.36	5.54	5.07	5.10	5.60	6.06
Residual Roof Drift (in.)	3.02	0.58	0.76	1.03	1.37	1.62	0.55	0.60	0.82	1.17	1.41	0.53	0.54	0.69	1.06	1.27
Max. Floor Drift (in.)	6.25	3.44	3.72	4.28	4.76	5.09	3.63	3.51	3.96	4.49	4.85	4.09	3.57	3.75	4.27	4.66
Residual Floor Drift (in.)	2.64	0.50	0.63	0.90	1.20	1.40	0.46	0.51	0.72	1.03	1.24	0.54	0.46	0.61	0.92	1.15
Total Base Shear (kips)	854	832	837	877	909	920	929	864	890	932	947	1079	927	904	946	966
Kobe																
Max. Rope Force (kips)	n/a	122	120	112	104	98	132	134	130	124	118	136	144	142	136	132
Max. Roof Drift (in.)	7.13	5.25	5.70	6.02	6.30	6.55	4.73	5.28	5.68	6.04	6.35	4.28	4.91	5.39	5.80	6.17
Residual Roof Drift (in.)	1.61	0.43	0.56	0.60	0.71	0.90	0.32	0.44	0.51	0.60	0.75	0.25	0.32	0.44	0.52	0.67
Max. Floor Drift (in.)	5.14	3.82	4.11	4.30	4.48	4.67	3.43	3.81	4.07	4.30	4.56	3.06	3.53	3.86	4.17	4.45
Residual Floor Drift (in.)	1.29	0.34	0.40	0.45	0.54	0.69	0.25	0.32	0.41	0.43	0.39	0.21	0.28	0.34	0.38	0.54
Total Base Shear (kips)	808	883	887	877	868	863	892	909	905	900	898	883	915	922	925	928
Near Field - Synthetic																
Max. Rope Force (kips)	n/a	276	254	252	252	234	346	318	294	287	277	410	374	344	317	322
Max. Roof Drift (in.)	11.95	9.1	9.18	9.27	9.27	9.6	8.67	8.82	8.96	9.11	9.2	8.25	8.46	8.68	8.87	8.99
Residual Roof Drift (in.)	1.76	1.1	1.14	1.02	1.01	1.04	0.96	1.21	1.11	1.05	1	0.84	1.06	1.2	1.11	1.04
Max. Floor Drift (in.)	8.76	7.3	7.11	7.48	7.48	7.75	7.28	7.1	6.93	7.33	7.6	7.19	0.71	6.89	6.88	7.4
Residual Floor Drift (in.)	1.3	0.94	0.92	0.87	0.87	0.9	0.83	0.99	0.91	0.92	0.93	0.73	0.9	1	0.94	0.92
Total Base Shear (kips)	936	1343	1287	1304	1304	1272	1504	1431	1361	1377	1363	1642	1556	1474	1410	1451

Average Values - Near Field Events

Max. Rope Force (kips)	n/a	169	160	159	158	150	209	191	183	182	176	252	223	207	199	200
Max. Roof Drift (in.)	9.11	6.49	6.68	7.01	7.29	7.62	6.18	6.38	6.67	7.02	7.30	6.02	6.15	6.39	6.76	7.07
Residual Roof Drift (in.)	2.13	0.70	0.82	0.88	1.03	1.19	0.61	0.75	0.81	0.94	1.05	0.54	0.64	0.78	0.90	0.99
Max. Floor Drift (in.)	6.72	4.85	4.98	5.35	5.57	5.84	4.78	4.81	4.99	5.37	5.67	4.78	2.60	4.83	5.11	5.50
Residual Floor Drift (in.)	1.74	0.59	0.65	0.74	0.87	1.00	0.51	0.61	0.68	0.79	0.85	0.49	0.55	0.65	0.75	0.87
Total Base Shear (kips)	866	1019	1004	1019	1027	1018	1108	1068	1052	1070	1069	1201	1133	1100	1094	1115

Table 3. 10: Far Field Event Results of Parametric Rope Analyses

	Frame Only	3 Ropes					4 Ropes					5 Ropes				
Initial Gap (in.)	n/a	0.2	0.4	0.6	0.8	1.0	0.2	0.4	0.6	0.8	1.0	0.2	0.4	0.6	0.8	1.0

Imperial Valley

Max. Rope Force (kips)	n/a	112	102	82	68	54	162	136	108	82	66	200	168	134	100	78
Max. Roof Drift (in.)	5.66	5.61	5.60	5.54	5.49	5.45	5.60	5.61	5.56	5.52	5.47	5.57	5.61	5.57	5.52	5.49
Residual Roof Drift (in.)	0.53	0.28	0.31	0.28	0.33	0.37	0.34	0.31	0.24	0.27	0.32	0.35	0.30	0.24	0.22	0.26
Max. Floor Drift (in.)	3.66	3.66	3.56	3.53	3.54	3.55	3.77	3.64	3.48	3.50	3.52	3.87	3.71	3.52	3.46	3.49
Residual Floor Drift (in.)	0.41	0.25	0.27	0.27	0.29	0.32	0.31	0.27	0.23	0.26	0.29	0.30	0.27	0.22	0.23	0.26
Total Base Shear (kips)	763	979	929	893	861	832	1073	1005	933	894	858	1162	1079	989	923	882

Chile

Max. Rope Force (kips)	n/a	111	90	68	52	38	144	118	88	64	48	170	146	108	78	58
Max. Roof Drift (in.)	5.34	5.30	5.17	5.06	5.01	5.07	5.26	5.21	5.06	4.97	5.03	5.10	5.23	5.05	4.95	5.00
Residual Roof Drift (in.)	0.87	0.35	0.46	0.47	0.58	0.70	0.41	0.40	0.41	0.49	0.67	0.33	0.41	0.37	0.45	0.64
Max. Floor Drift (in.)	3.36	3.51	3.28	3.17	3.13	3.19	3.50	3.33	3.18	3.11	3.16	3.43	3.38	3.18	3.09	3.14
Residual Floor Drift (in.)	0.69	0.44	0.38	0.36	0.46	0.59	0.38	0.38	0.35	0.40	0.57	0.30	0.38	0.34	0.36	0.53
Total Base Shear (kips)	708	958	890	838	808	783	1024	952	880	834	803	1075	1015	920	856	823

Far Field - Synthetic

Max. Rope Force (kips)	n/a	176	174	158	146	136	202	208	196	174	164	240	230	228	204	186
Max. Roof Drift (in.)	7.63	6.17	6.43	6.65	6.79	6.95	5.89	6.17	6.46	6.62	6.78	5.76	5.93	6.3	6.48	6.65
Residual Roof Drift (in.)	1.23	0.1	0.35	0.47	0.5	0.6	0	0	0.2	0.4	0.5	0.3	0	0	0.13	0.3
Max. Floor Drift (in.)	5.79	4.75	4.93	5.17	5.3	5.39	4.67	4.71	4.99	5.17	5.31	4.71	4.57	4.85	5.06	5.22
Residual Floor Drift (in.)	1.18	0.23	0.5	0.6	0.7	0.7	0	0.4	0.47	0.65	0.65	0.12	0.13	0.3	0.4	0.6
Total Base Shear (kips)	856	1173	1164	1163	1147	1127	1251	1213	1218	1203	1185	1338	1260	1260	1249	1231

Average Values - Far Field Events

Max. Rope Force (kips)	n/a	133	122	103	89	76	169	154	131	107	93	203	181	157	127	107
Max. Roof Drift (in.)	6.21	5.69	5.73	5.75	5.76	5.82	5.58	5.66	5.69	5.70	5.76	5.48	5.59	5.64	5.65	5.71
Residual Roof Drift (in.)	0.88	0.24	0.37	0.41	0.47	0.56	0.25	0.24	0.28	0.39	0.50	0.33	0.24	0.20	0.27	0.40
Max. Floor Drift (in.)	4.27	3.97	3.92	3.96	3.99	4.04	3.98	3.89	3.88	3.93	4.00	4.00	3.89	3.85	3.87	3.95
Residual Floor Drift (in.)	0.76	0.31	0.38	0.41	0.48	0.54	0.23	0.35	0.35	0.44	0.50	0.24	0.26	0.29	0.33	0.46
Total Base Shear (kips)	775	1037	994	965	939	914	1116	1057	1010	977	949	1192	1118	1056	1009	979

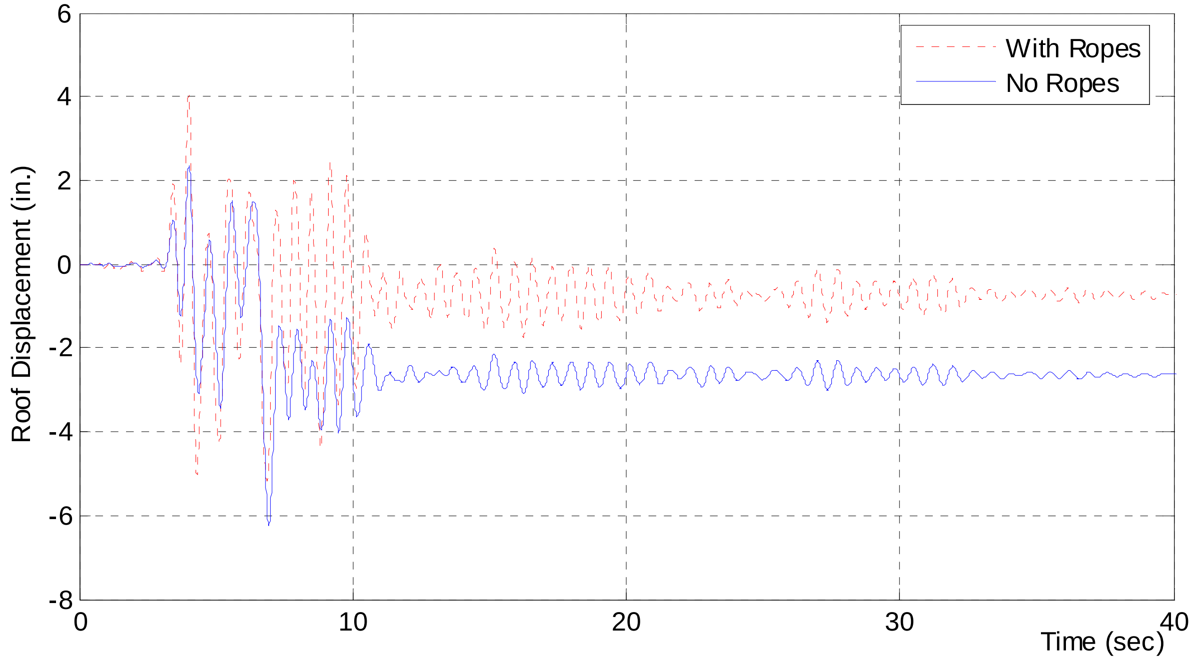

a) Comparison of Frame with Ropes versus Frame without Ropes

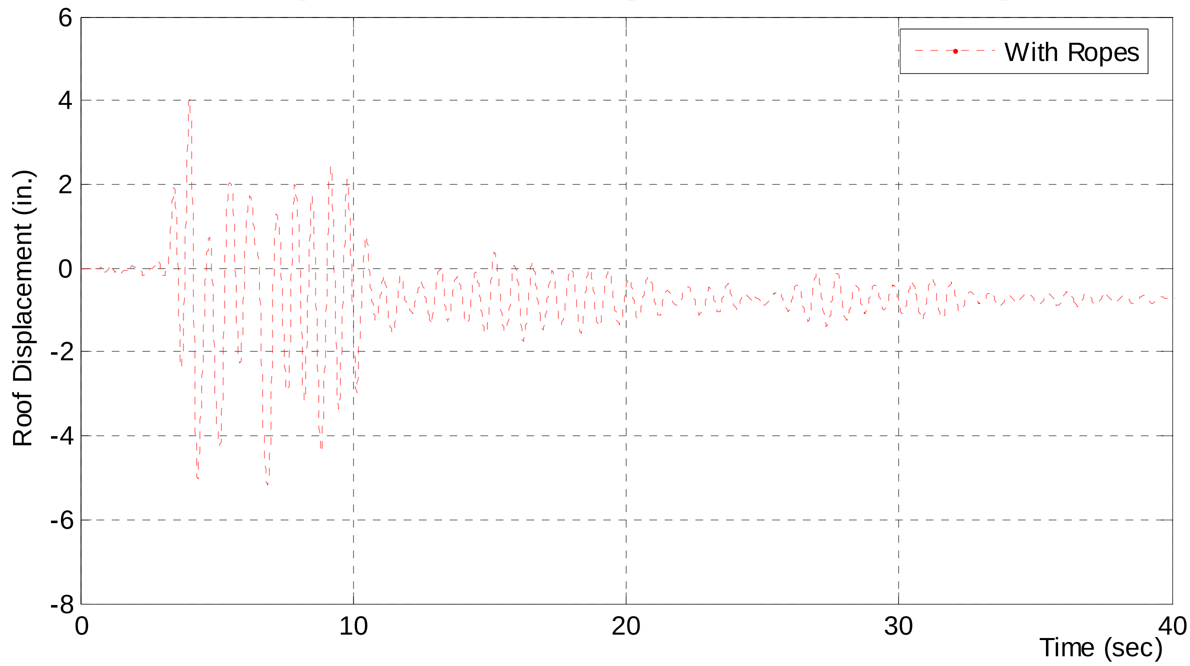

b) Frame without Ropes Shown Separately for Clarity

Figure 3. 9: Roof Displacement History: Northridge

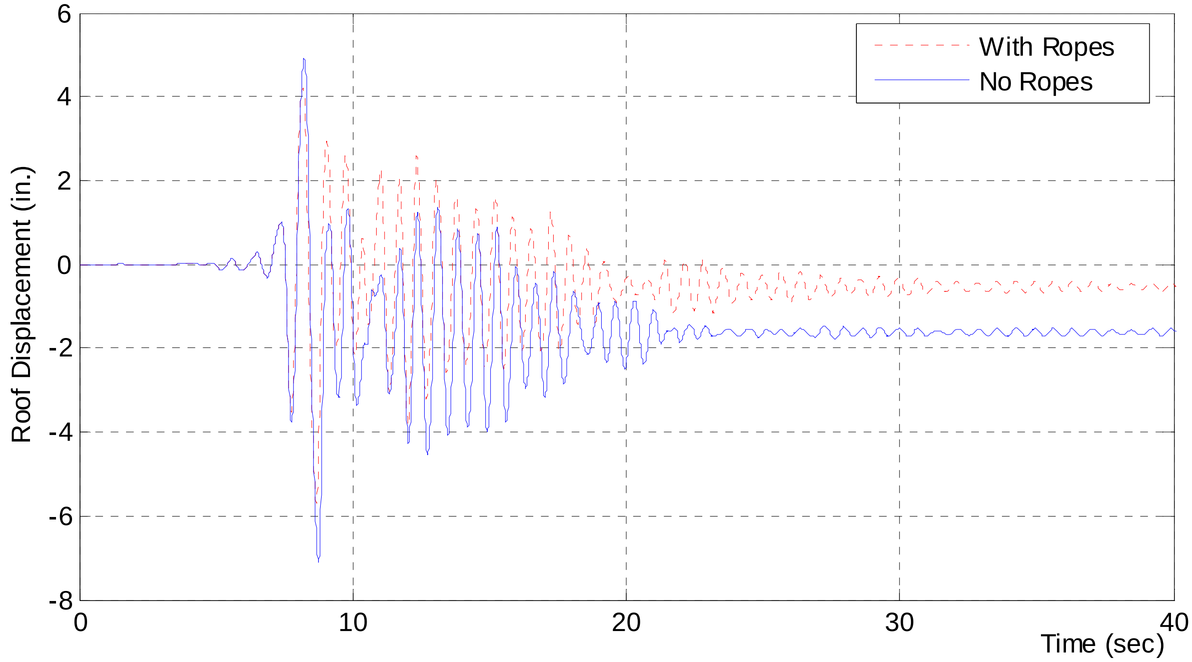

a) Comparison of Frame with Ropes versus Frame without Ropes

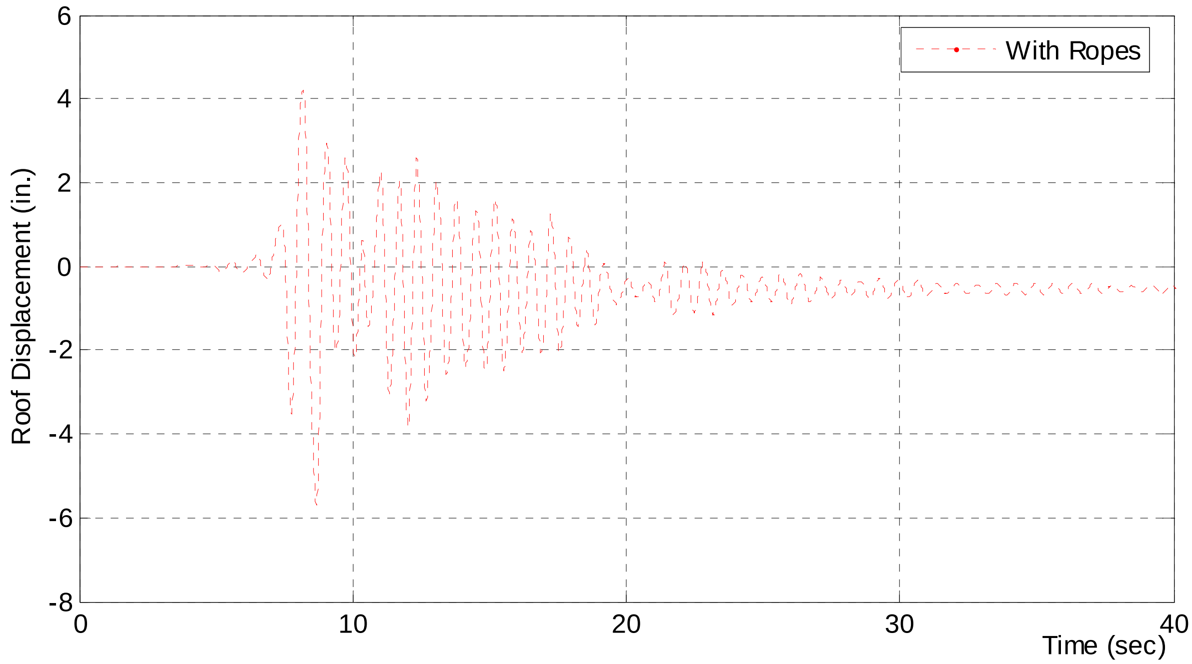

b) Frame without Ropes Shown Separately for Clarity

Figure 3. 10: Roof Displacement History: Kobe

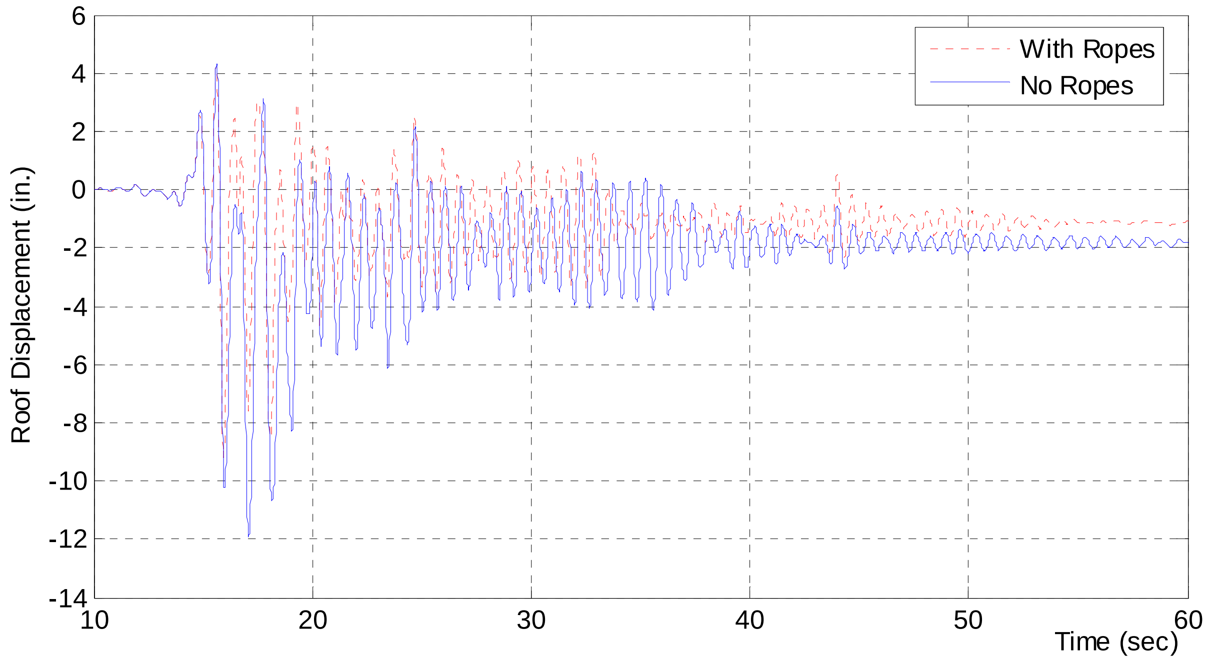

a) Comparison of Frame with Ropes versus Frame without Ropes

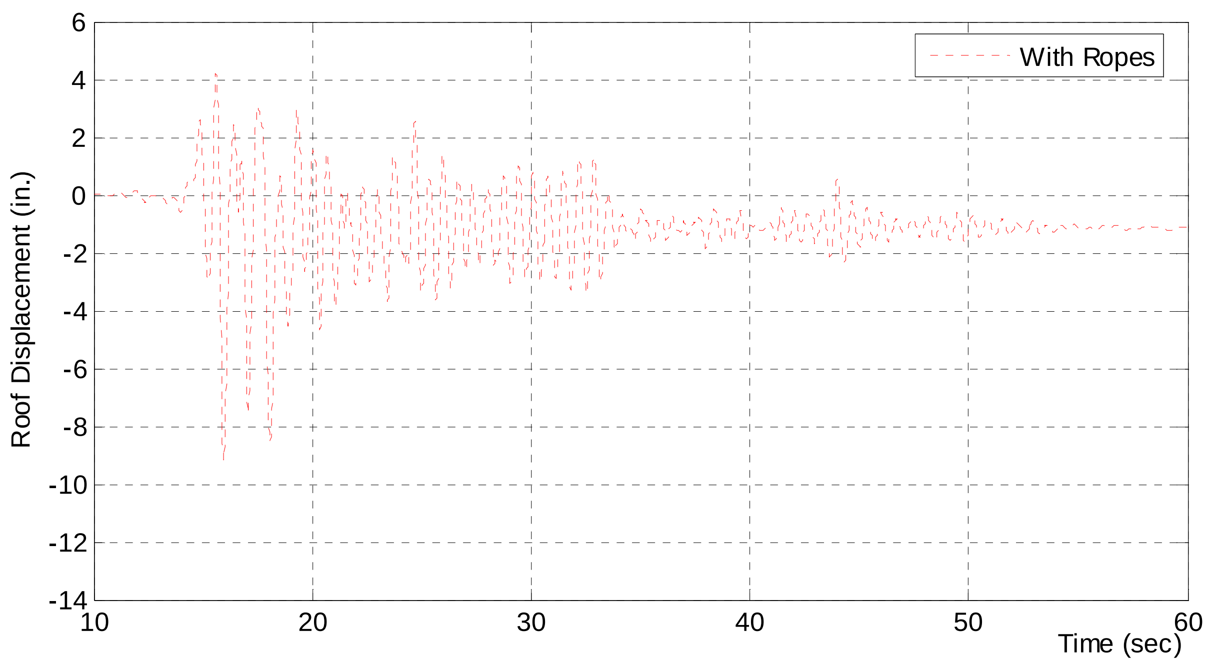

b) Frame without Ropes Shown Separately for Clarity

Figure 3. 11: Roof Displacement History: Synthetic – Near Field

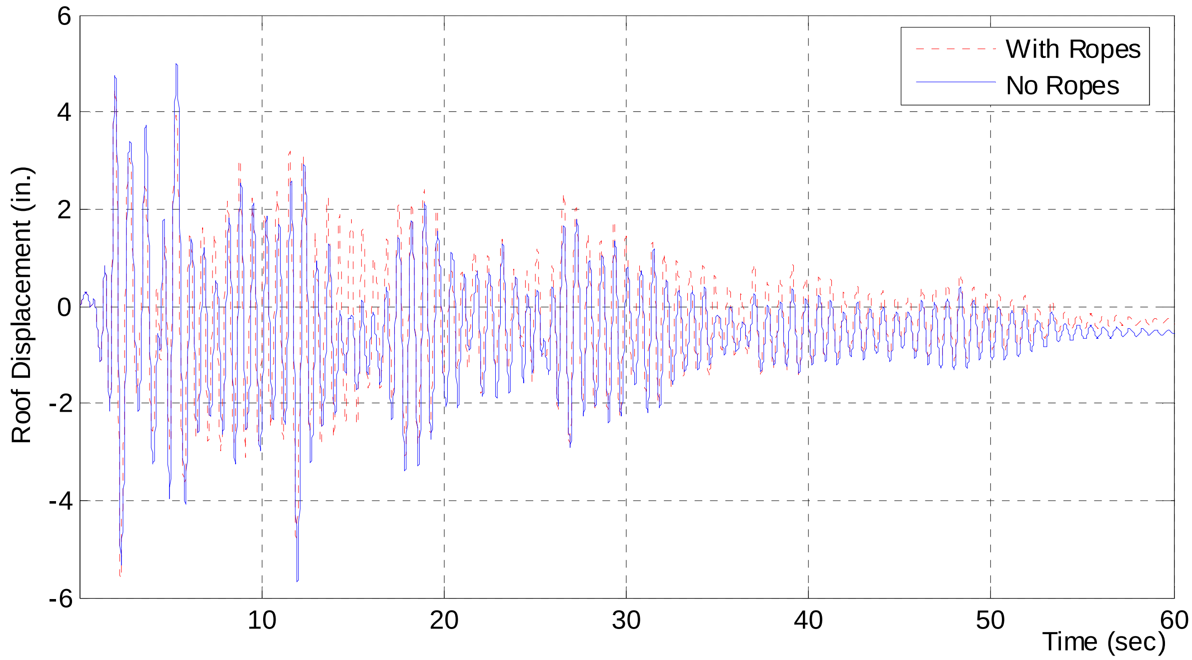

a) Comparison of Frame with Ropes versus Frame without Ropes

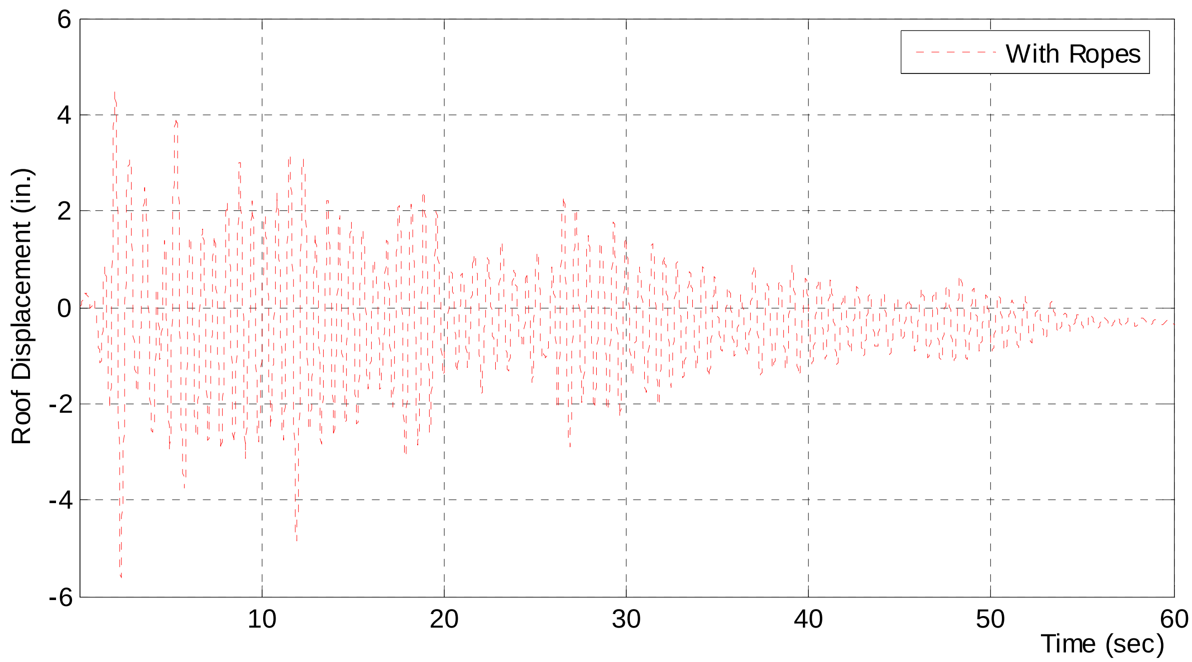

b) Frame without Ropes Shown Separately for Clarity

Figure 3. 12: Roof Displacement History: Imperial Valley

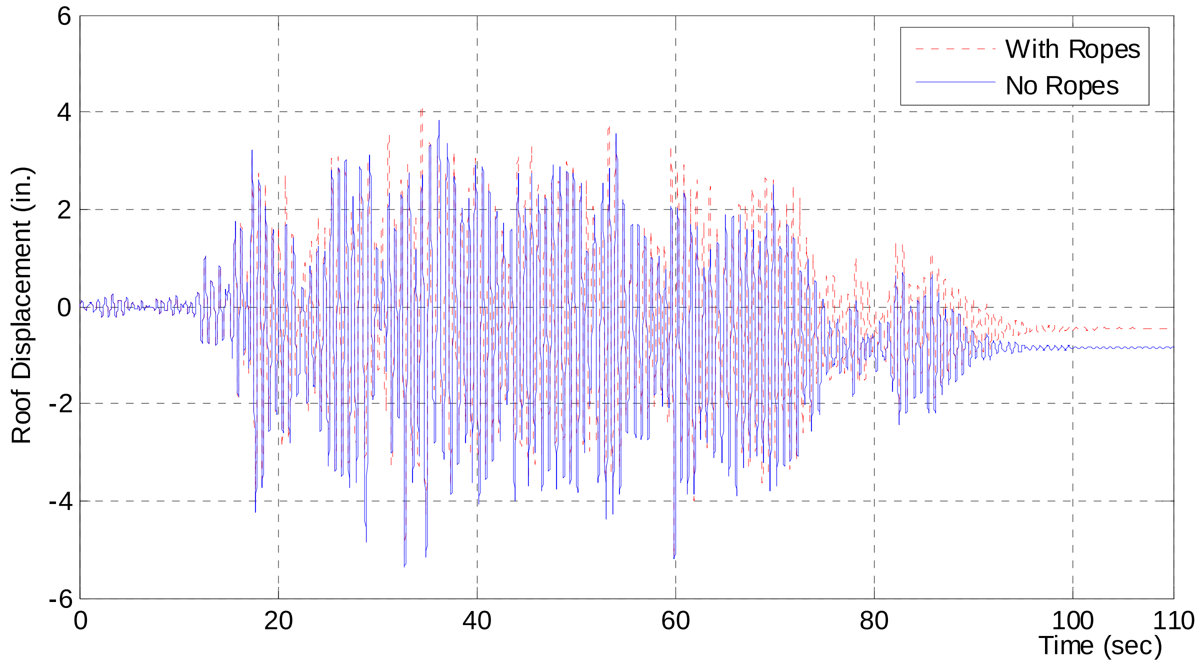

a) Comparison of Frame with Ropes versus Frame without Ropes

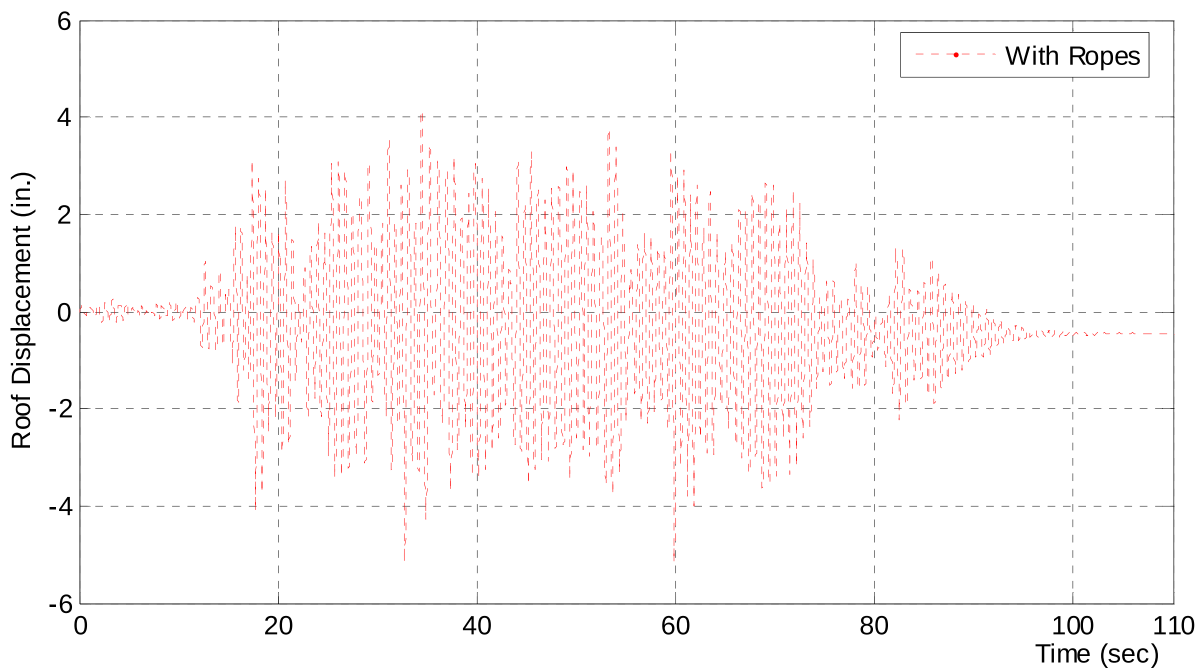

b) Frame without Ropes Shown Separately for Clarity

Figure 3. 13: Roof Displacement History: Chile

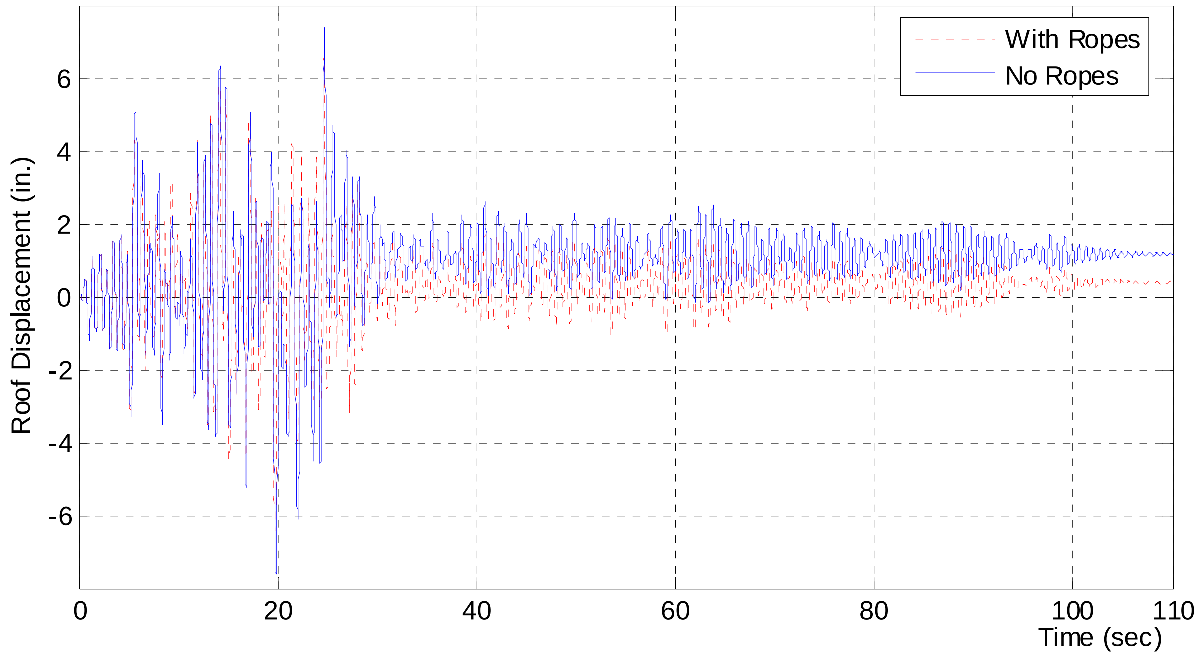

a) Comparison of Frame with Ropes versus Frame without Ropes

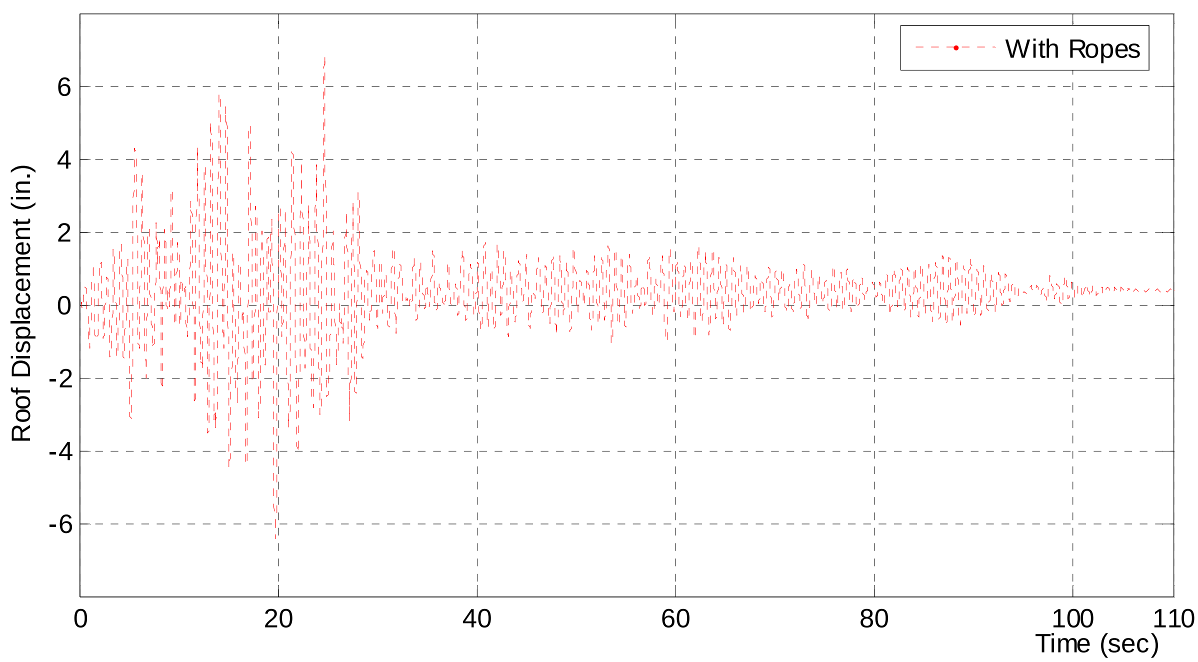

b) Frame without Ropes Shown Separately for Clarity

Figure 3. 14: Roof Displacement History: Far Field - Synthetic

The mean response parameters of interest for the prototype frame, with and without the selected prototype rope response, are listed in Tables 3.11 and 3.12 for near and far field ground motion suites, respectively. Percent change in response parameters of interest between the frame with and without ropes was calculated as follows:

$$\text{Percent Change} = \frac{RP_{NR} - RP_{WR}}{RP_{NR}} \text{ x } 100\% \tag{3-17}$$

where RP_{NR} is the response parameter of the frame without ropes and RP_{WR} is the response parameter of the frame with ropes.

Table 3. 11: Mean Percent Change in Response Parameters: Near-Field Events

Response Parameters	**Prototype Frame**	**Frame with 3-rope, 0.4-in.-gap device**	**Percent Change**
Max Rope Force (kips)	n/a	160	n/a
Max Roof Drift(in.)	9.11	6.68	- 26.6
Residual Roof Drift (in.)	2.13	0.82	- 61.5
Max Floor Drift (in.)	6.72	4.98	- 25.9
Residual Floor Drift (in.)	1.74	0.65	- 62.6
Total Base Shear (kips)	866	1004	+ 15.9

Table 3. 12: Mean Percent Change in Response Parameters: Far-Field Events

Response Parameters	**Prototype Frame**	**Frame with 3-rope, 0.4-in.-gap device**	**Percent Change**
Max Rope Force (kips)	n/a	122	n/a
Max Roof Drift(in.)	6.21	5.73	- 7.73
Residual Roof Drift (in.)	0.88	0.37	- 58.0
Max Floor Drift (in.)	4.27	3.92	- 8.19
Residual Floor Drift (in.)	0.76	0.38	- 50.0
Total Base Shear (kips)	776	994	+ 28.1

3.6 INTERMEDIATE TUBE STEEL FRAME

An intermediate full-scale, single-bay, tube steel moment frame, which approximated the dynamic response characteristics of the full-scale, five-bay, wide-flange prototype moment frame, was developed and analyzed as an intermediate step in the development of a 1:6-scale frame. The resulting intermediate moment frame is shown in Figure 3.15. The shaking table load limit was the primary consideration for initial proportioning of the intermediate moment frame. Final member sizes and mass definitions were then chosen based on matching the first and second resonant frequencies of the prototype.

A study was conducted to determine the maximum weight of the scaled model that could be excited with the shaking table using the Northridge ground motion, and is presented in Appendix B. Based on ballast tests it was determined that 4,700 lbs was the maximum weight of a scale-model for which Northridge ground motion input could be precisely controlled. Using this limit, the total maximum scale frame mass (m_{TS}) was calculated as follows:

$$\text{Total Scale Frame Mass} = m_{TS} = \frac{W}{g} = \frac{4.700 \ \text{kips}}{386.4 \ \frac{\text{in.}}{\text{sec}^2}} = 0.0122 \frac{\text{k} - \text{sec}^2}{\text{in.}} \qquad (3\text{-}18)$$

The correlating total intermediate moment frame mass was found by multiplying the total scale-frame mass by the mass scale factor (λ_M):

$$m_{TI} = (m_{TS})(\lambda_M) = (0.0122)(5.78^2) = 0.408 \frac{\text{k} - \text{sec}^2}{\text{in.}} \qquad (3\text{-}19)$$

The total intermediate moment frame mass corresponds to approximately 10% of the total mass tributary to one five-bay moment frame of the prototype structure.

To proportion an intermediate frame with first and second resonant frequencies similar to those of the five-bay prototype, a frame with approximately ten percent of the initial stiffness of the prototype was found by trial and error. The iterative process consisted of choosing tube steel sections for the intermediate frame and developing plastic hinge responses for the members using the methodology outlined in Section 4.1.2. The stiffness of the intermediate moment frame was compared to the stiffness of the prototype frame, based on push-over analyses. It was determined that using HSS16x8x5/16-A500 column sections and HSS14x4x3/8-A500 beam sections would result in a frame having approximately ten percent of the initial stiffness of the prototype. Mass definitions for the intermediate frame were proportioned such that 78.2 % of the total mass was placed at the floor level and 21.8% of the total mass was placed at the roof level, based on the floor-to-roof mass ratios of the prototype structure. The total mass was then adjusted slightly until the first and second resonant frequencies of the prototype and intermediate moment frames were reasonably similar.

A comparison of first and second resonant frequencies for the prototype and intermediate moment frames is shown in Table 3.13. A comparison of the pushover curve for the moment frames is illustrated in Figure 3.16. A comparison of the roof displacement history for each frame when subjected to nonlinear, response history analyses in DRAIN is shown for the Northridge acceleration input and for the Imperial Valley acceleration input in Figures 3.17 and 3.18, respectively. It is clear that the single-bay, tube steel, intermediate moment frame represents the dynamic response characteristics of the prototype moment frame. Therefore, a meaningful reduction to a 1:6-scale tube steel moment frame structure from the prototype can be made by applying similitude principles to the intermediate moment frame.

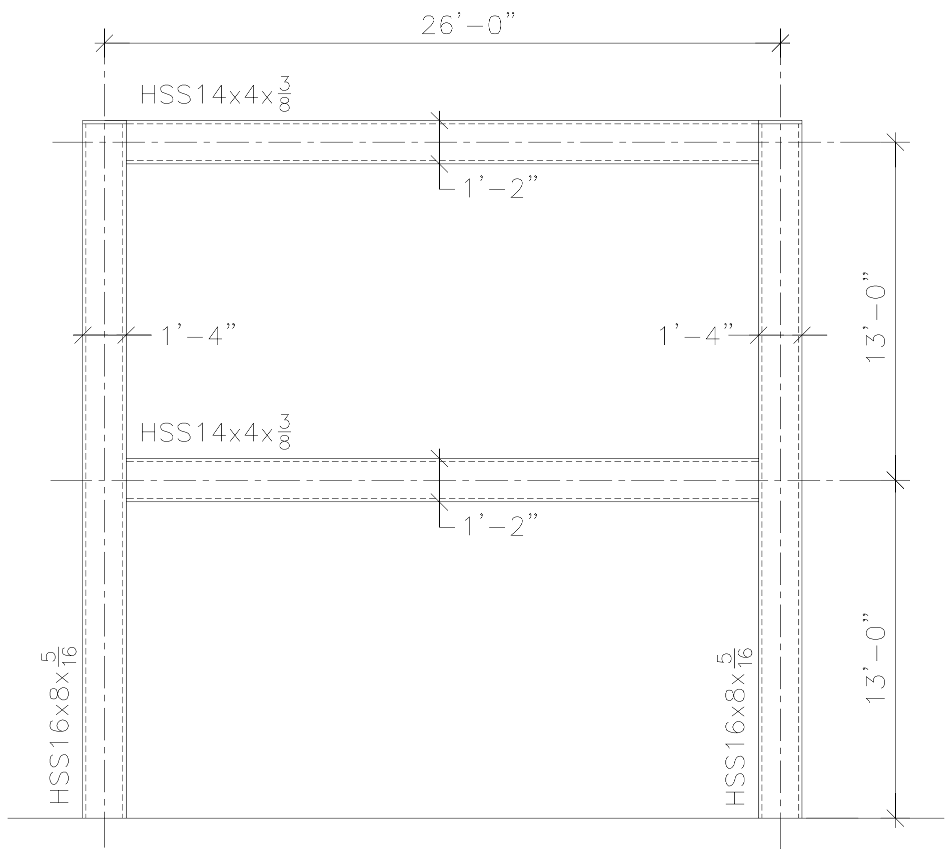

Figure 3. 15: Intermediate Moment Frame

Table 3. 13: Resonant Periods of Vibration Comparison

	Prototype Frame	**Single-Bay Intermediate Frame**
T_1 (seconds)	0.70	0.71
T_2 (seconds)	0.23	0.22

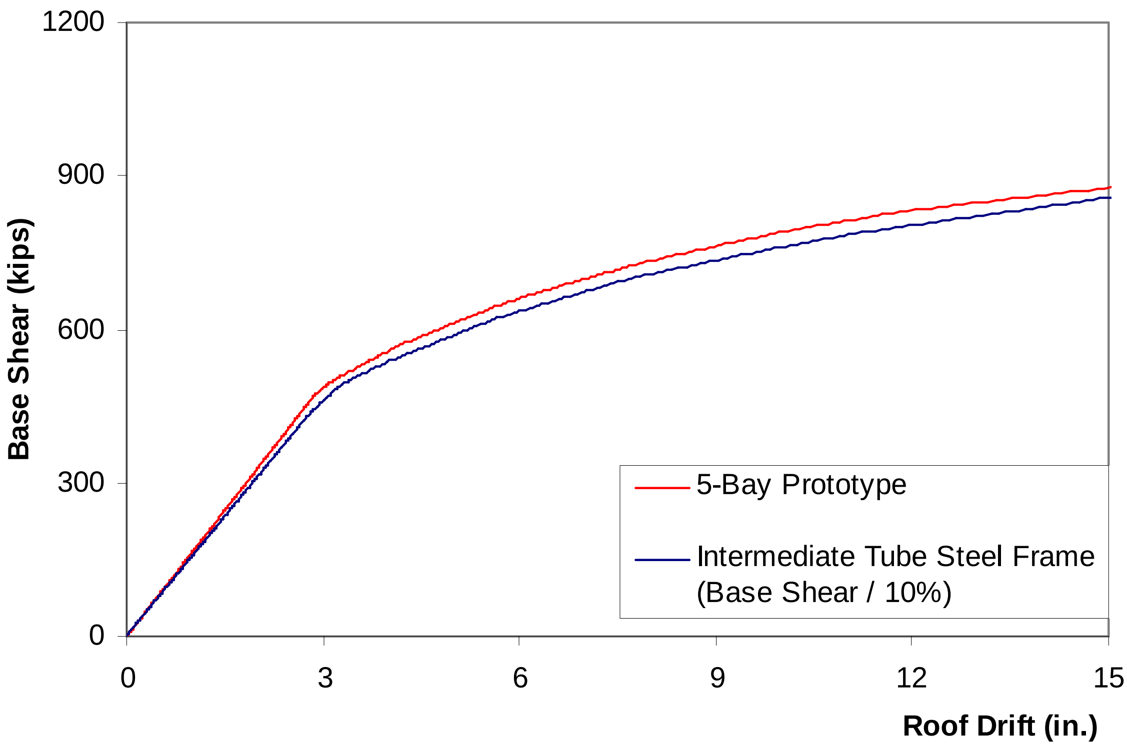

Figure 3. 16: Pushover Curve Comparison

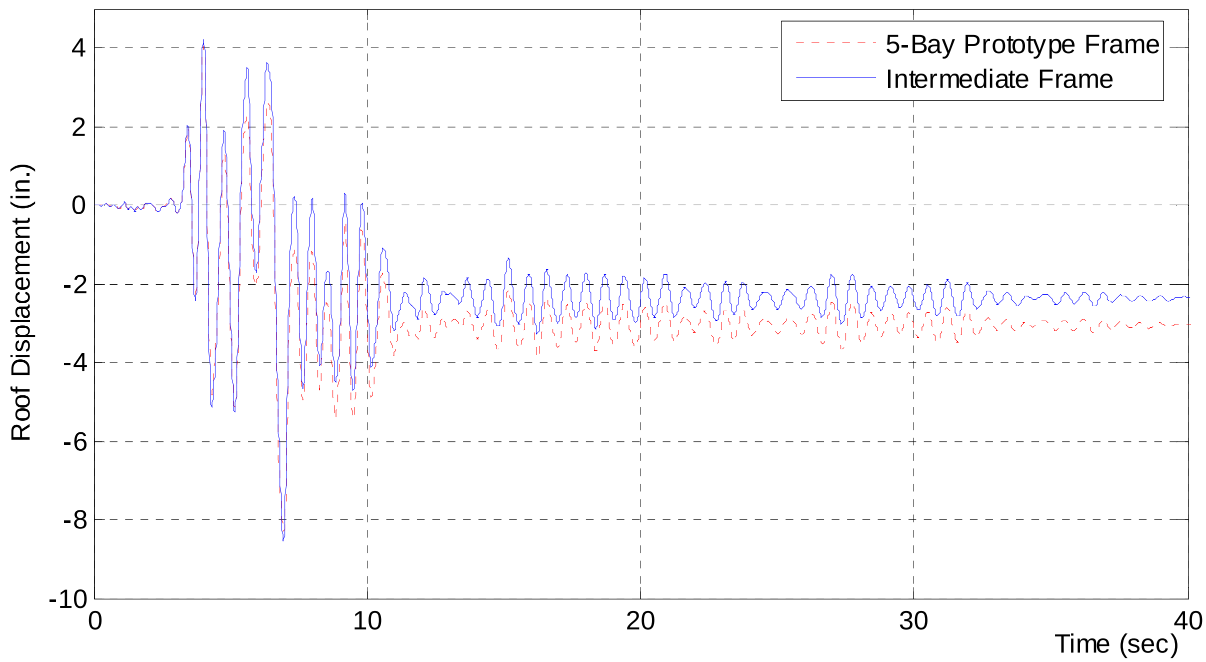

a) Prototype and Intermediate Frame Comparison

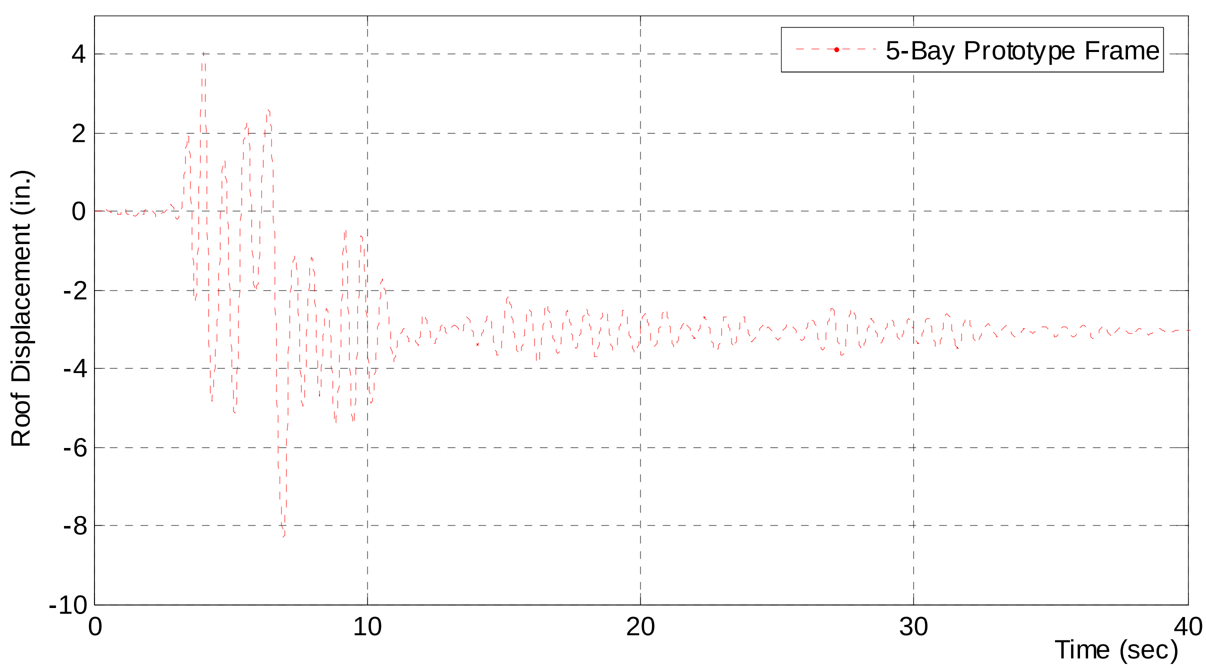

b) Prototype Frame Shown Separately for Clarity

Figure 3. 17: Roof Displacement Comparison of Prototype and Intermediate Moment Frames: Northridge Ground Motion

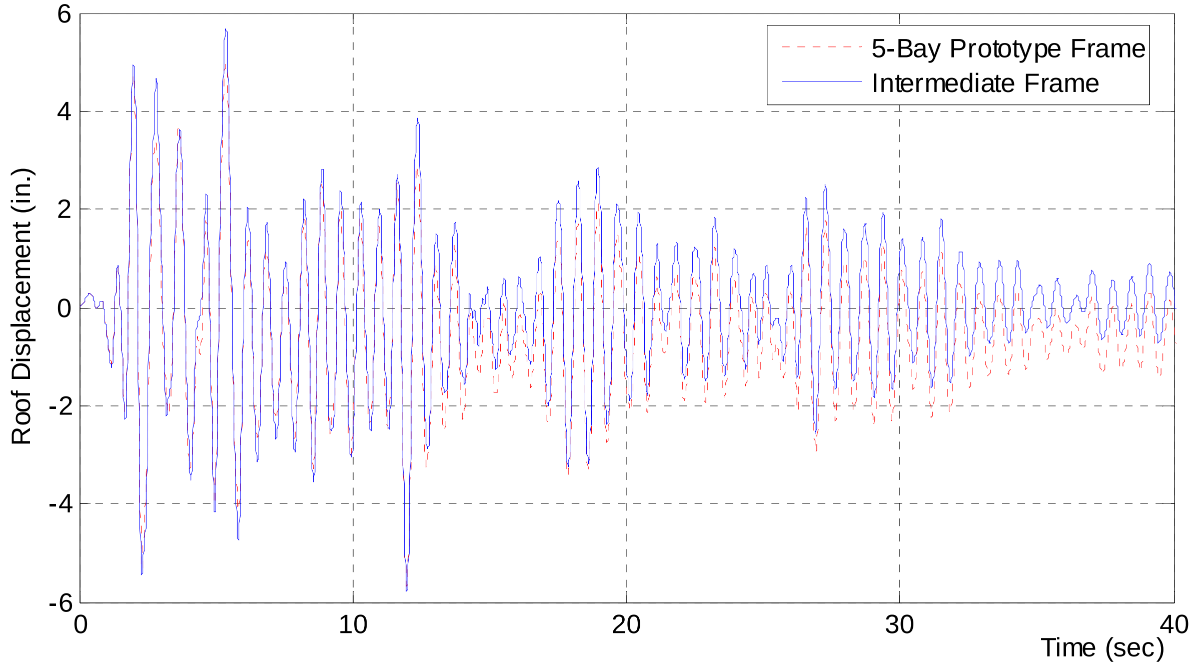

a) Prototype and Intermediate Frame Comparison

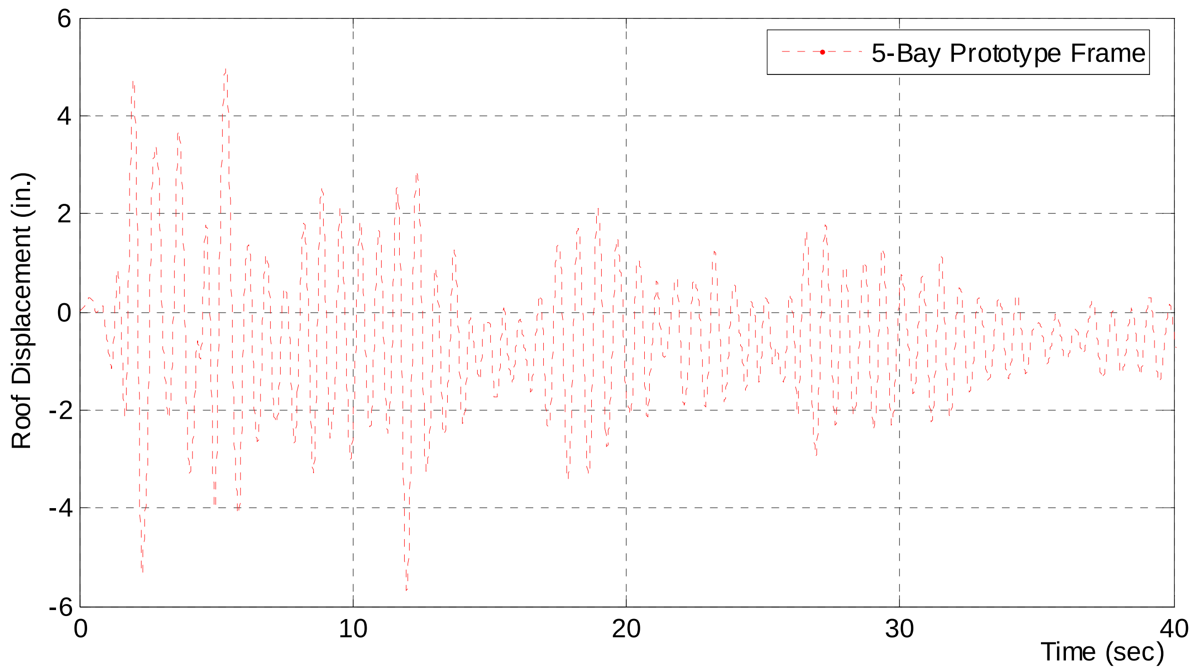

c) Prototype Frame Shown Separately for Clarity

Figure 3. 18: Roof Displacement Comparison of Prototype and Intermediate Moment Frames: Imperial Valley Ground Motion

3.7 1:6-SCALE MODEL

3.7.1 1:6-SCALE MOMENT FRAME

Based on similitude principles, outlined in Appendix C, a 1:6-scale frame was developed for shaking table experiments by dividing the overall dimensions of the intermediate moment frame, the bending stiffness of the intermediate moment frame members, and mass at the diaphragm levels of the intermediate moment frame by appropriate scaling factors listed in Table 3.14. Intermediate moment frame parameters, scaling factors, corresponding target 1:6-scale frame parameters, and actual frame parameters for the 1:6-scale moment frame are shown in Table 3.14. The resulting 1:6-scale frame is illustrated in Figure 3.19. Since standard HSS shapes were intended for use in the 1:6-scale frame, precisely matching the target bending stiffness listed in Table 3.14 was not possible. Consequently, the 1:6-scale frame mass was adjusted slightly to match the target resonant periods of vibration of the intermediate frame.

The 1:6-scale moment frame was modeled in DRAIN as described in Section 3.4 and subjected to Northridge and Imperial Valley ground motion acceleration history files. Time for the ground motions was scaled by λ_T, listed in Table 3.14. Acceleration values were not scaled, since scaling factors were developed with acceleration kept constant between the full-scale and the 1:6-scale model. A comparison of the roof displacement histories for the five-bay prototype moment frame and the 1:6-scale moment frame resulting from nonlinear, response history analyses conducted using DRAIN are shown in Figure 3.20 for the Northridge acceleration input and Figure 3.21 for Imperial Valley acceleration input. It should be noted that time and displacement data from the 1:6-scale frame analyses were converted to the full scale for comparison with the five-bay prototype response. This was accomplished by multiplying the displacement results and the corresponding time values from the DRAIN simulation for the 1:6-scale frame by λ_L and λ_T, respectively.

Table 3. 14: Scale Frame Parameters

Parameters	Intermediate Frame	Scaling Factor	Value for Scaling Factor	Target Scale Frame Values	Actual Scale Frame Values
Frame Width (in.)	312	λ_L	5.78	54	54
Story Height (in.)	156	λ_L	5.78	27	27
Column Bending Stiffness (in.^{4})	451	λ_L^4	1164	0.387	0.406
Beam Bending Stiffness (in.^{4})	252	λ_L^4	1164	0.216	0.188
Mass at FloorLevel (k-sec.^{2} / in.)	0.274	λ_M	33.4	$8.06\text{x}10^{-3}$	$8.00\text{x}10^{-3}$
Mass at Roof (k-sec.^{2} / in.)	0.096	λ_M	33.4	$2.87\text{x}10^{-3}$	$2.24\text{x}10^{-2}$
T_1 (seconds)	0.70	λ_T	2.40	0.29	0.29
T_2 (seconds)	0.22	λ_T	2.40	0.09	0.09

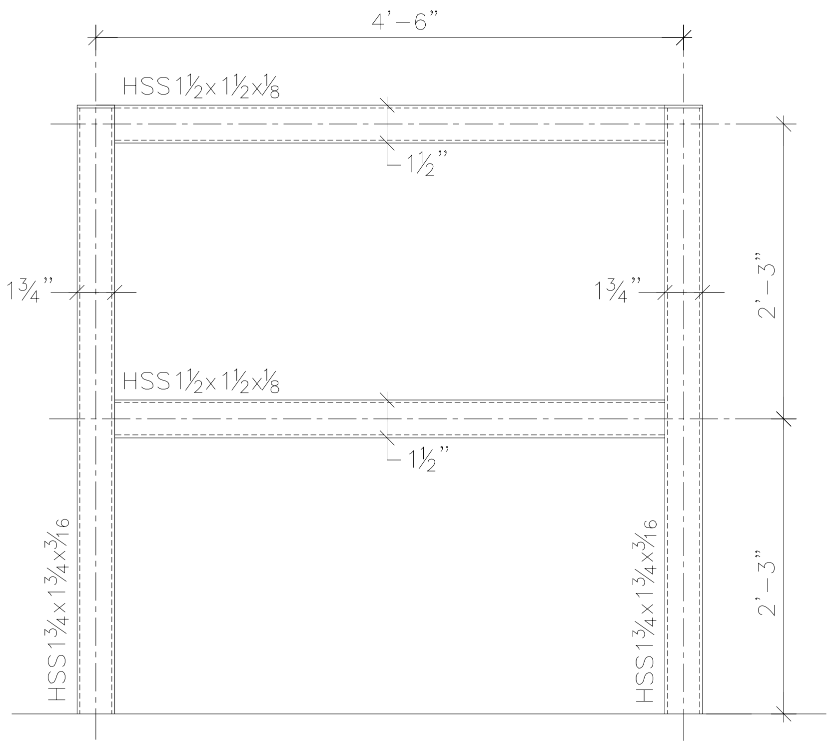

Figure 3. 19: 1:6-Scale Moment Frame

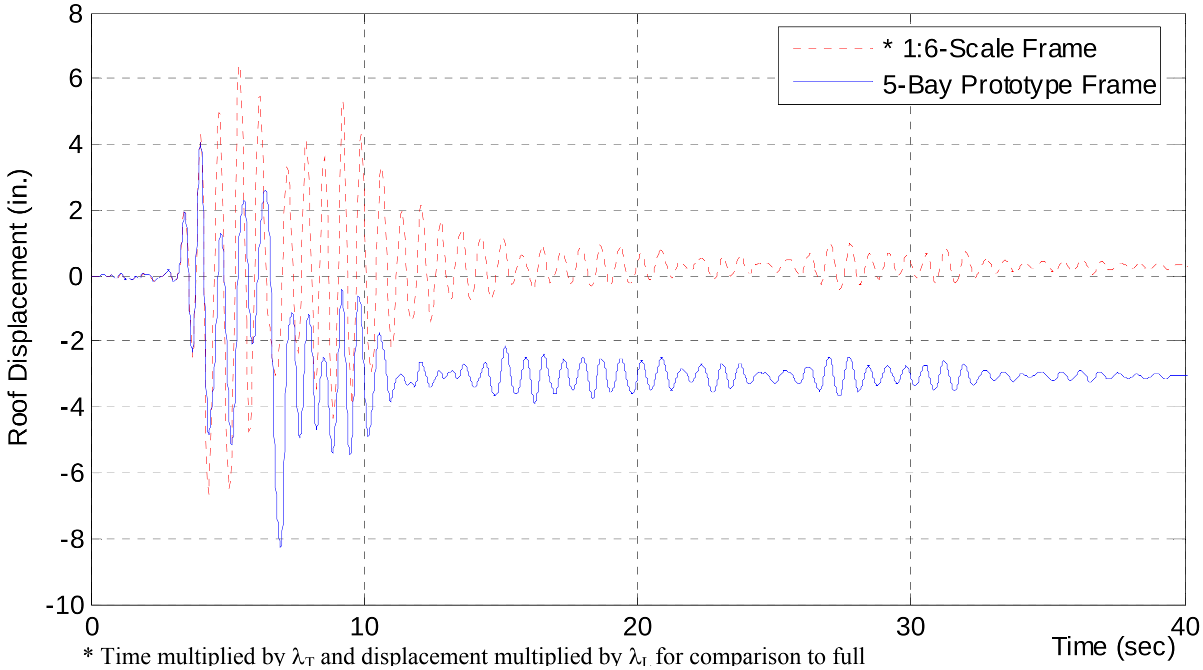

a) Prototype and 1:6-Scale Frame Comparison

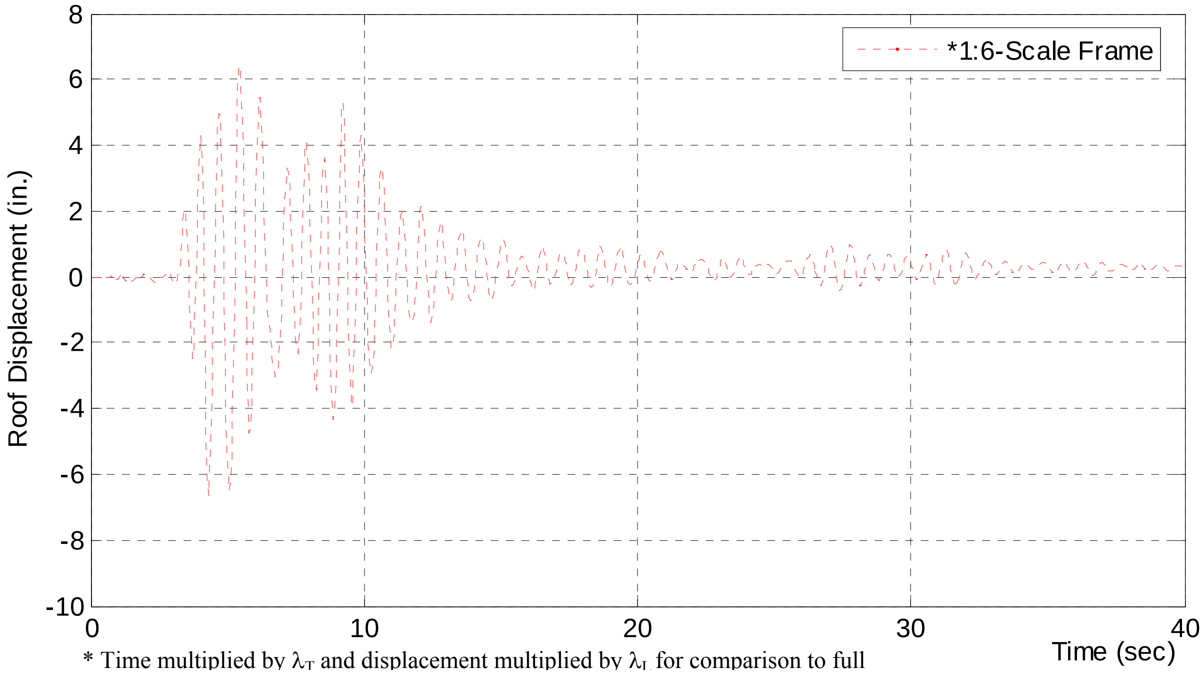

b) 1:6-Scale Frame Shown Separately for Clarity

Figure 3. 20: Comparison of Prototype and 1:6-Scale Frame Displacements: Northridge

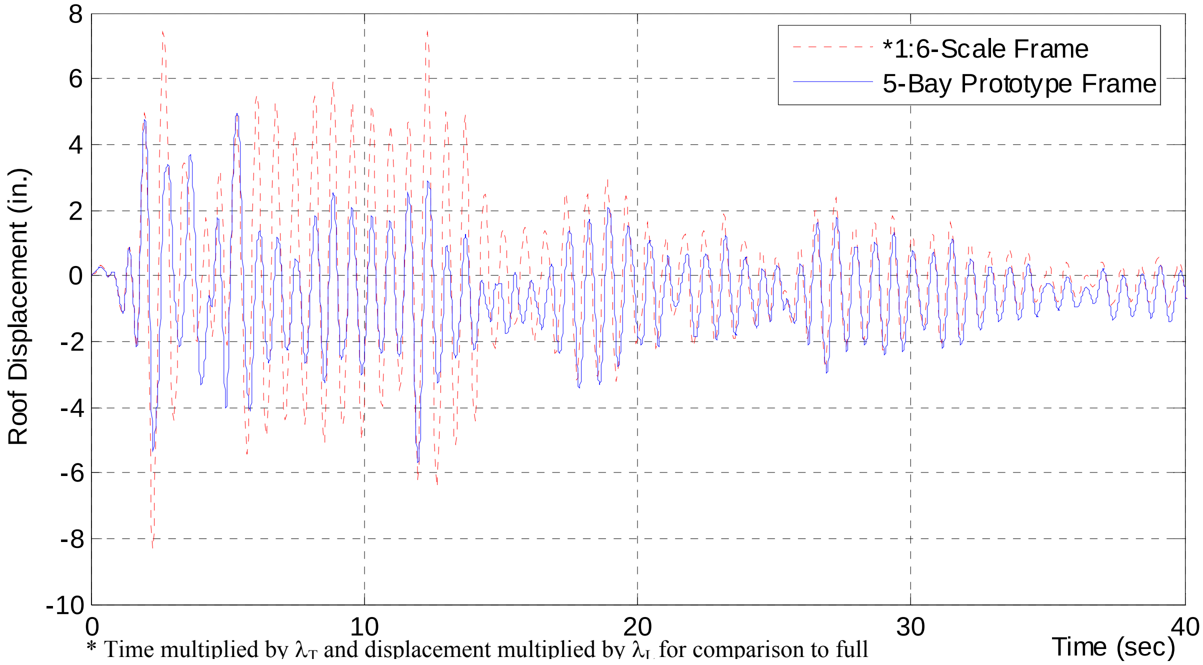

a) Prototype and 1:6-Scale Frame Comparison

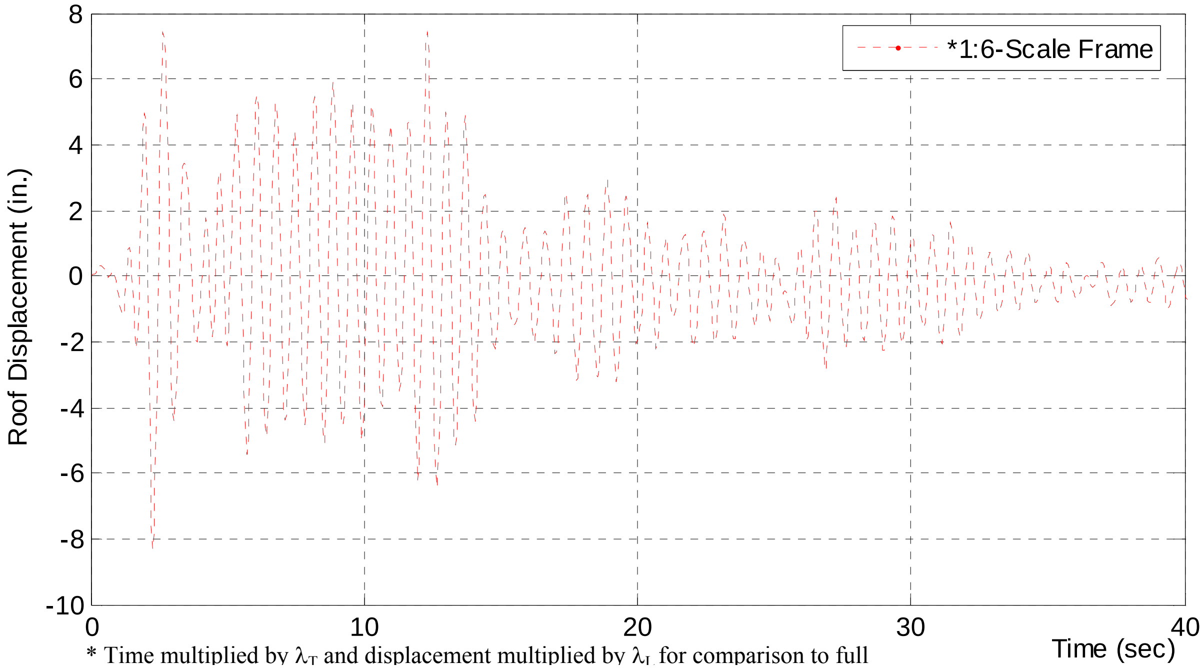

b) 1:6-Scale Frame Shown Separately for Clarity

Figure 3. 21: Comparison of Prototype and 1:6-Scale Frame Displacements: Imperial Valley

In both comparisons, it was observed that the displacement histories were not consistent throughout the time domain. In particular, it was clear that very little residual drift was predicted for the 1:6-scale frame subjected to the Northridge event. This inconsistency is a result of the ratio of the 1:6-scale frame member depths to the prototype member depths being approximately 1:12. The increase in the member depth scaling factor resulted in an increased elastic rotational capacity of the shallower member, requiring greater drift prior to yielding. The inconsistency in results is not due to improper scaling of overall frame dimensions, elastic member stiffness, mass, or time. To demonstrate the accuracy of appropriate scaling without plasticity, the plastic hinges of the five-bay prototype and 1:6-scale frame models were removed, and the response history analyses were repeated using the Northridge ground-motion acceleration. Displacements at the roof and floor level were recorded for each frame and are shown in Figures 3.22 and 3.23, respectively. The roof and floor response histories are nearly identical, indicating that the model was scaled properly.

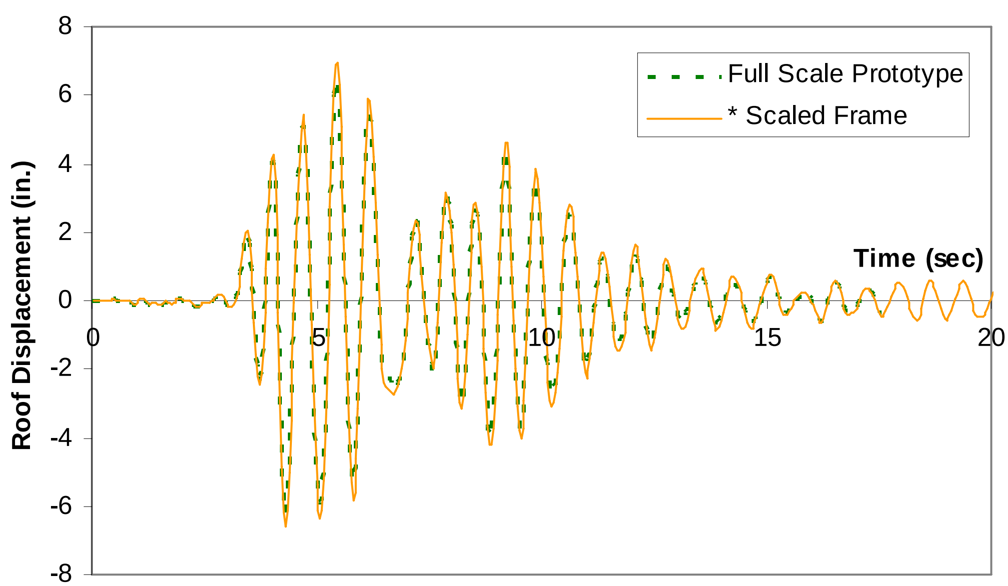

* Time multiplied by λ_T and displacement multiplied by λ_L for comparison to full scale

Figure 3. 22: Elastic Roof Displacement History Comparison: Northridge

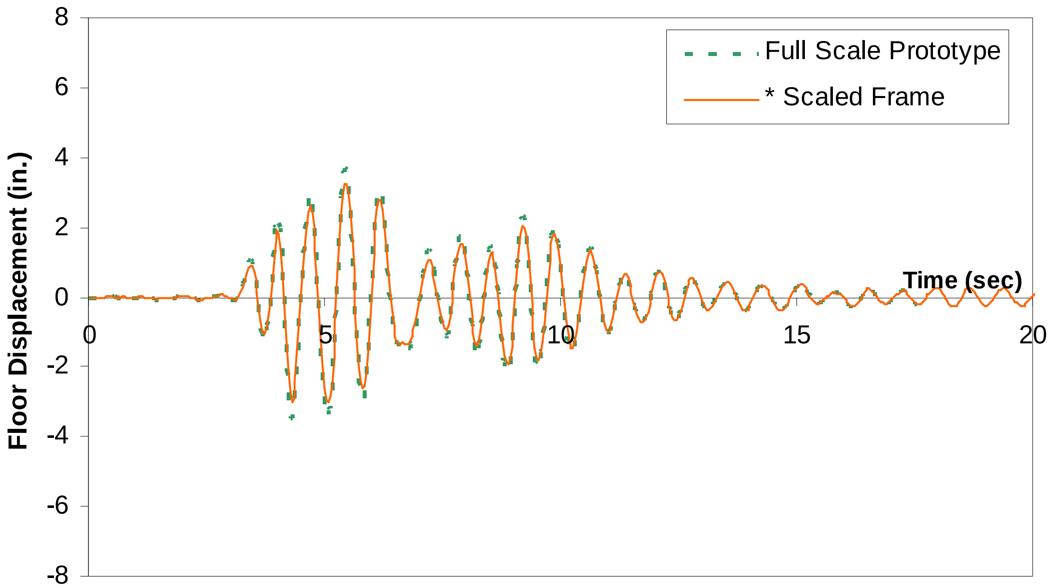

* Time multiplied by λ_T and displacement multiplied by λ_L for comparison to full scale

Figure 3. 23: Elastic Floor Displacement History Comparison: Northridge

However, since control of post-yield drift was the focus of this study, the 1:6-scale moment frame needed to be re-evaluated. Two options were considered: use of deeper members for the 1:6-scale frame, or increase of the magnitude of the input acceleration to force plastic hinge formation in the scale frame. Using a deeper member with a properly scaled bending stiffness required the use of non-standard, built-up member sections. The process of fabricating such frame members was determined to be infeasible. Option two was explored by re-analyzing the 1:6-scale frame in DRAIN and incrementally increasing the intensity of the Northridge ground motion. The residual drift of the 1:6-scale frame matched the residual drift approximated for the five-bay prototype when the Northridge ground-motion acceleration input was multiplied by 1.80 as seen in Figure 3.24.

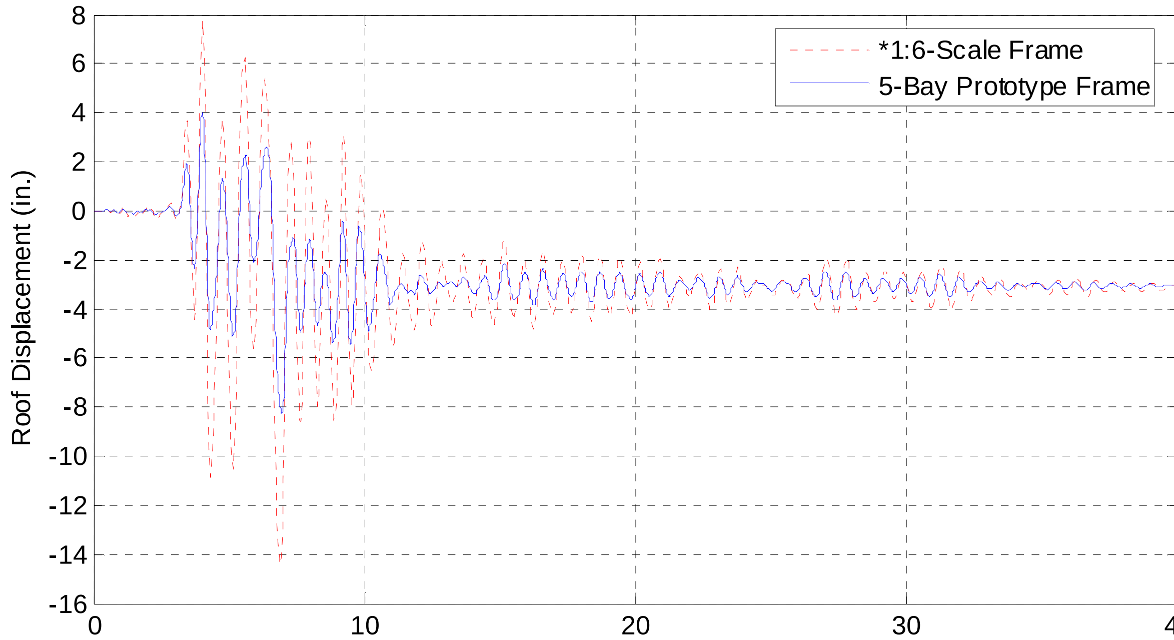

* Time multiplied by λ_T and displacement multiplied by λ_L for comparison to full

a) Prototype and 1:6-Scale Frame Comparison

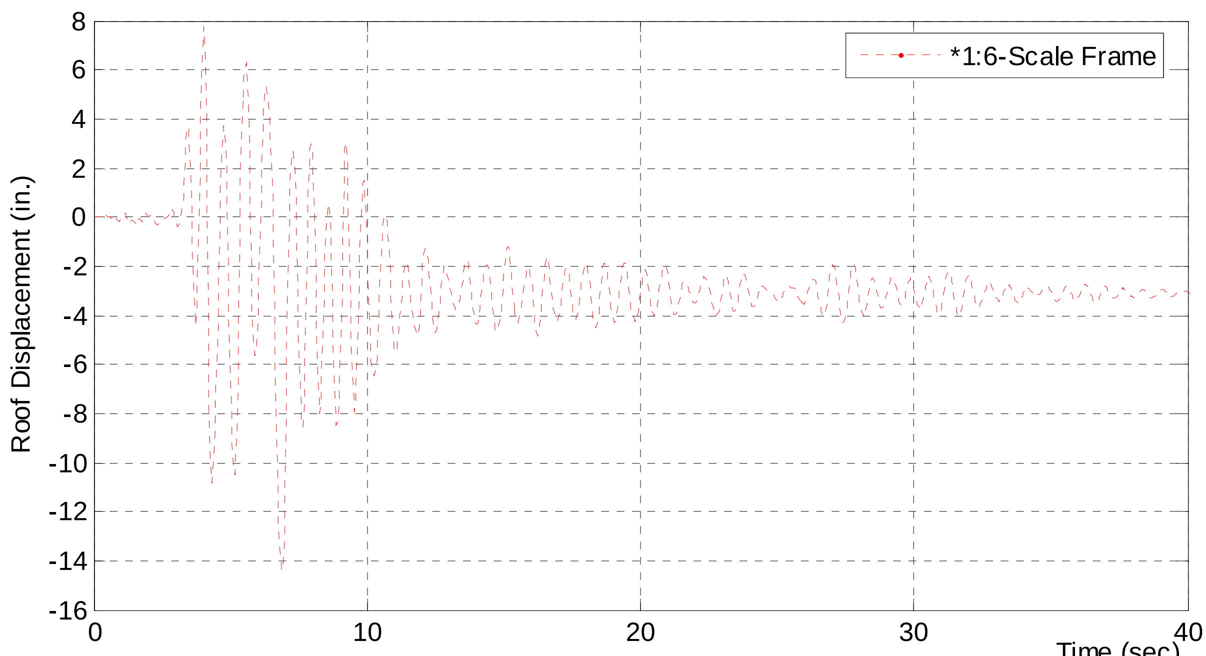

* Time multiplied by λ_T and displacement multiplied by λ_L for comparison to full

b) 1:6-Scale Frame Shown Separately for Clarity

Figure 3. 24: Scale Frame Roof Displacement History Comparison
(Scaled Northridge Ground Motion Accelerations Increased by 80%)

3.7.2 SCALED ROPE MODEL

A DRAIN study was conducted to determine the response of the 1:6-scale frame with properly scaled rope elements added. A scaled-rope model definition was determined based on the full-scale rope model definitions shown in Figure 3.6 and similitude principles.

Multiples of the rope response exhibited by a 1-in. nominal diameter, 8-ft-long Amsteel II rope were studied to determine the most effective response for a the full-scale, five-bay prototype during the parametric study documented in Section 5.5. It was determined that a response representing three ropes at each of three diagonal elements, with an initial gap equal to 0.4 in., produced the most desirable results. The response across the diagonal was defined using the following values:

Initial Stiffness:	k1 = 0.00 kips / in.
Secondary Stiffness:	k2 = 39.30 kips / in.
Tertiary Stiffness:	k3 = 82.00 kips / in.
Initial Stiffness Displacement Limit:	u1 = 0.40 in.
Secondary Stiffness Displacement Limit:	u2 = 1.30 in.

The stiffness values for k2 and k3 were increased 300% to account for three diagonal rope elements being represented by a single diagonal in the 1:6-scale moment frame. Since the mass and stiffness of the 1:6-scale moment frame represented 10% of the total mass and stiffness of the five-bay prototype, the rope stiffness values were also multiplied by 0.1. Resulting rope stiffness values are:

Secondary Stiffness:	k2 = 11.79 kips / in.
Tertiary Stiffness:	k3 = 24.60 kips / in.

The stiffness values and displacement limit values were then converted to the 1:6-scale stiffness values as follows:

$$k_{SCALE} = \left(k_{PROTO.}\right)\frac{\lambda_L}{\lambda_{FORCE}} = \left(k_{PROTO.}\right)\frac{\lambda_L}{\lambda_L^2} = \left(k_{PROTO.}\right)\frac{1}{\lambda_L} \qquad (3\text{-}20)$$

$$u_{SCALE} = \left(u_{PROTO.}\right)\frac{1}{\lambda_L} \tag{3-21}$$

The response across the diagonal for the 1:6-scale rope was therefore defined using the following values:

Initial Stiffness:	k1 = 0.00 kips / in.
Secondary Stiffness:	k2 = 2.04 kips / in.
Tertiary Stiffness:	k3 = 4.26 kips / in.
Initial Stiffness Displacement Limit:	u1 = 0.07 in.
Secondary Stiffness Displacement Limit:	u2 = 0.22 in.

The diagonal elements were added to the scale frame model in DRAIN and a nonlinear response history simulation was repeated using the scaled Northridge ground motion record. A comparison of the roof drift history of the frame with ropes is compared to the drift history without ropes in Figure 5.21. The relative reduction in total drift and residual drift is observed to be consistent with the reductions observed for the full-scale prototype roof displacement history.

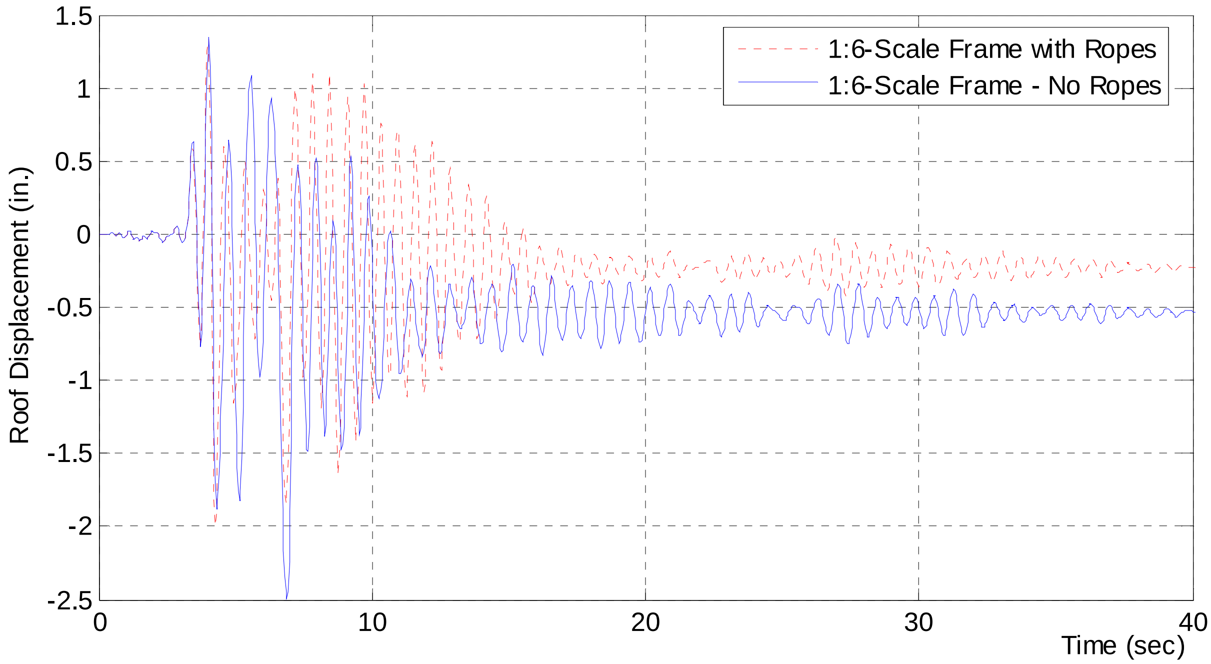

a) Comparison of 1:6-Scale Frame with and without Ropes

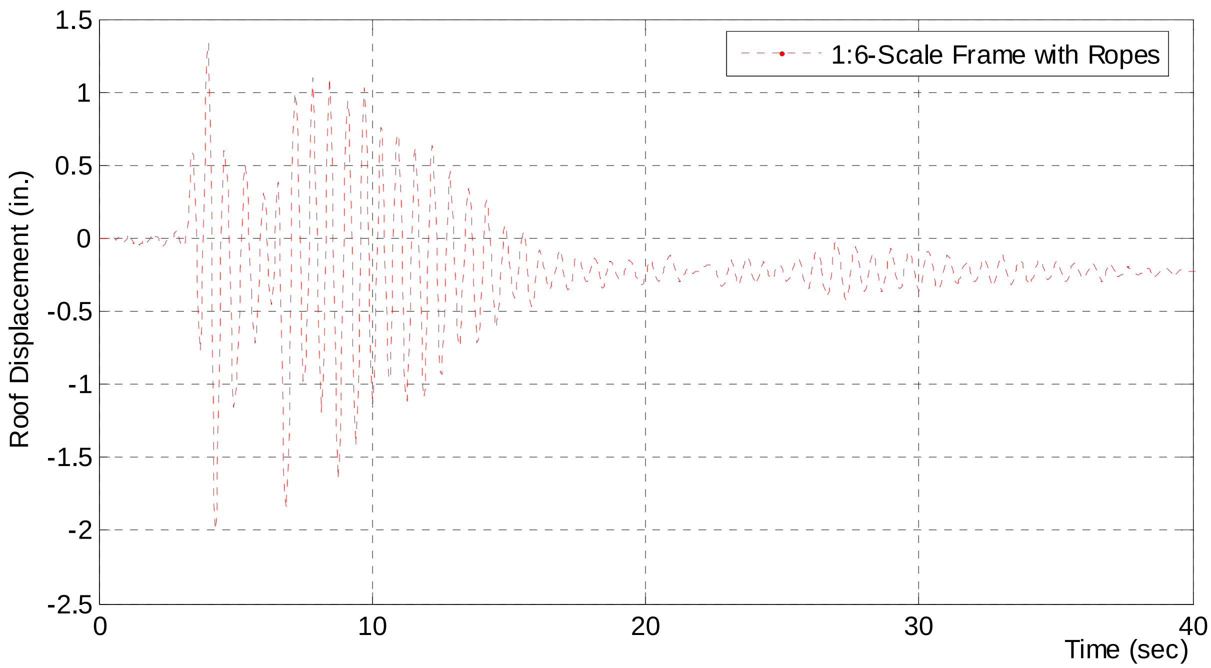

b) 1:6-Scale Frame Shown Separately for Clarity

Figure 3. 25: Displacement History Comparison of Scaled Frame with and Without Ropes (Scaled Northridge Ground Motion Accelerations Increased by 80%)